π^0 PHOTOPRODUCTION FROM THE DEUTERON AT FORWARD ANGLES IN THE ENERGY RANGE FROM 900 MEV TO 1400 MEV

Thesis by
Carl R. Clinesmith

In Partial Fulfillment of the Requirements

For the Degree of
Doctor of Philosophy

California Institute of Technology
Pasadena, California
1967
(Submitted January 25 , 1967)

ACKNOWLEDGMENTS

This experiment was supervised by Professor Alvin V. Tollestrup. By his teaching I have made the transition from working book problems to doing experimental research. It is difficult to properly acknowledge also those things learned not from pedagogy but by example. The guidance of Professor Robert Walker in all phases of my graduate career has been invaluable. The continuing interest of Professor Robert Bacher is appreciated.

The total experiment using hydrogen and deuterium targets was performed in collaboration with G. Laurie Hatch. The division of labor and material did not come about until the actual writing of the two theses. As such, the methods and results reported are his as much as mine.

My first interaction with synchrotron physics was as an apprentice to Professor Richard Talman. Many of my attitudes were formed from working with him. From his days as a student, consultation with Professor Charles Peck has been useful. To him, and also to Drs. Joe Mullins and Owen Maloy, goes the credit for making the Phase III Synchrotron a working, 1500 MeV machine. Conversation with Drs. Donald Coyne, Stanley Ecklund, and Professor Donald Groom, while we were fellow students, made the solving of many problems a more pleasant task. Most of my knowledge of the theoretical aspects of photoproduction is the result of conversation with Dr. Jean Hebb.

The hydrogen - deuterium target was designed by Mr. Earle Emery, and was constructed and maintained by him and by Mr. Richard Wileman. The Synchrotron crew, headed by Larry Loucks, and the

machine operators Al Neubeiser, Frank Scarlino and Joe Laurinovics, are of course essential to all experiments.

Most of the mechanical apparatus was constructed by Walter A. Nilsson. I am also especially grateful to Phyllis Nilsson, who made a significant contribution during the final phase of my career as a student.

I would like to thank my wife Judy, my mother, the Woodrow Wilson Foundation, the IBM Corporation, the National Science Foundation, and the California Institute of Technology for financial support.

ABSTRACT

The cross section for the reaction $\gamma + d \rightarrow \pi^o + p + n$ was measured at the Caltech synchrotron. The π^o was detected by measuring its decay gamma rays with two lead glass, total absorption Cherenkov counters. The results are three angular distributions at k = 911, 1180, and 1390 MeV, at forward angles from 3 degrees to 90 degrees. The deuteron/proton ratio differs significantly from 2.0, but final state effects from the use of a deuteron target make impossible quantitative conclusions about the neutron cross section.

To Judy

TABLE OF CONTENTS

LIST OF TABLES

LIST OF FIGURES

I. INTRODUCTION

The single pion photoproduction reactions which can be measured in the laboratory are

1) $\gamma + p \rightarrow \pi^+ + n$

2) $\gamma + p \rightarrow \pi^o + p$

3) $\gamma + n \rightarrow \pi^- + p$

4) $\gamma + n \rightarrow \pi^o + n$

where the reactions from the neutron must use a deuteron target. A bremsstrahlung beam contains all incoming energies up to its maximum, so measurement of cross sections for the two particle final state requires identifying the particle and measuring its direction and energy. The ease and accuracy of magnetic spectrometer analysis make this method preferable whenever a charged particle is produced with sufficient energy. The magnetic spectrometer method has been used to measure π^+ and π^- photoproduction cross sections detecting the pion, and for π^o photoproduction from protons detecting the proton. The difficulty of detecting the low energy proton accompanying a π^o produced in the forward direction limits the magnetic spectrometer method to angles greater than about 50 degrees in our energy range. The desire to measure small angle π^o photoproduction from protons, as well as to measure the corresponding reaction from the neutron, leads to attempts to measure the π^o itself. Measurement of the π^o was made practical by the development of total absorption Cherenkov counters as gamma-ray spectrometers. These

counters allow measurement of the π^0 alone by detecting the two decay gamma rays in coincidence and recording their pulse heights. The counters were first used to measure π^0 production from complex nuclei in an attempt to measure the π^0 lifetime.[1] They were then used to measure cross sections for π^0 photoproduction from hydrogen in the forward direction.[2]

The increase in intensity of the CIT synchrotron, plus the reaching of its designed endpoint energy of 1500 MeV, led to redoing the previous measurements from hydrogen, extending the data to higher energy, and doing an identical set of measurements from deuterium. The work was carried out at three mean photon energies, 911, 1182, and 1390 MeV, at 10 degree intervals from 0 to 90 degrees. This thesis reports the investigation of deuterium. The simultaneous work on hydrogen is given in the thesis of G. Laurie Hatch.[3]

II. DESCRIPTION OF EXPERIMENTAL METHOD

The aim of the experiment is to measure the π^0 angular distribution in the reaction $\gamma + d \rightarrow \pi^0 + (p + n)$ by detecting the two decay gamma rays from the π^0 in lead glass Cherenkov counters.[4] Briefly, these counters detect the Cherenkov light produced by the electromagnetic shower in the lead glass initiated by the incident photon or electron. The size of the counters is sufficient to contain the entire shower. The Cherenkov light is collected by nine 5" RCA 7046 phototubes, the outputs of which are summed. The amount of Cherenkov light produced is directly proportional to the energy of the initiating particle, so the average pulse height produced is a linear function of the incident energy. The distribution in pulse height in the output of the counters from a beam of mono-energetic particles is approximately Gaussian. By testing with the mono-energetic electron beam the width of the distribution was found to correspond to production of about 200 photoelectrons per BeV. A non-shower producing particle such as a proton or cosmic ray muon passing through the counter produces the same amount of light as a 220 MeV electron. Since the average pulse height from the Cherenkov counter is a linear function of energy, the pulse height can be displayed in energy with just a scale change. We will use this scale throughout the thesis, usually depending upon the context to distinguish between reference to a particle energy or to a pulse height in the Cherenkov counter.

The experimental layout is shown in Figure 1. In the usual manner, the bremsstrahlung beam from the synchrotron is incident on the target which contains liquid hydrogen or liquid deuterium.

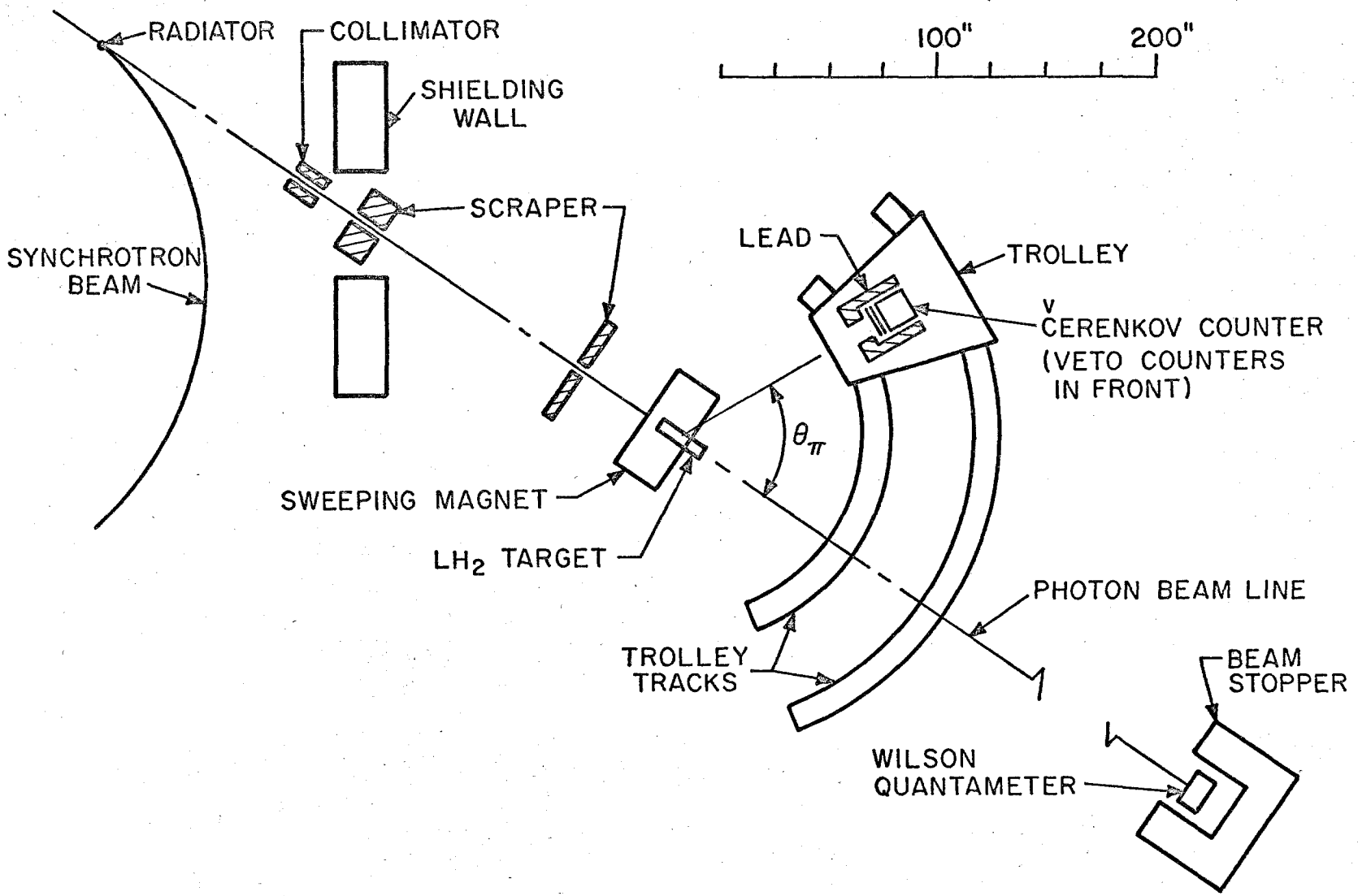

FIGURE 1 BEAM AREA LAYOUT

The beam is then monitored directly by a Wilson quantameter. The produced π^0's decay essentially at their point of production, and each decay gamma ray is seen by the apertures, shown in Figure 2. Given that we have seen the decay gamma rays of a single π^0, the kinematic variables which the system geometry defines are the pion direction and energy. In order to be able to detect both decay gamma rays, the pion direction must lie in the rectangle containing the apertures, which defines the θ and φ limits. To determine the energy limits of pions the system will detect, we consider the opening angle between the two decay gamma rays in the laboratory system. This angle has a minimum which increases with decreasing pion energy. The maximum angle subtended by the apertures then defines the minimum energy pion the system can detect, which we call E_G, the geometric cutoff energy. Having defined the angles by the setting, the maximum pion energy is given by the kinematics relation for the maximum photon energy. Hence the lead glass counter system will define the energy and angle acceptance without any reference to pulse-height information, although such reference will in fact be necessary to separate the reaction of interest from the detection of double π^0 production. With the system as used, the counter rectangle subtends a solid angle of about 20 millisteradians. The resolution function is chosen to sample the same photon energy limits by choosing the geometric cutoff energy to correspond to the same photon energy at all angles. The resolution function defined in this way has the same shape in photon energy at all angles.

The Cherenkov counters were mounted one above the other on a trolley which could be moved to any angle at a constant radius about the target. The counters could be moved independently

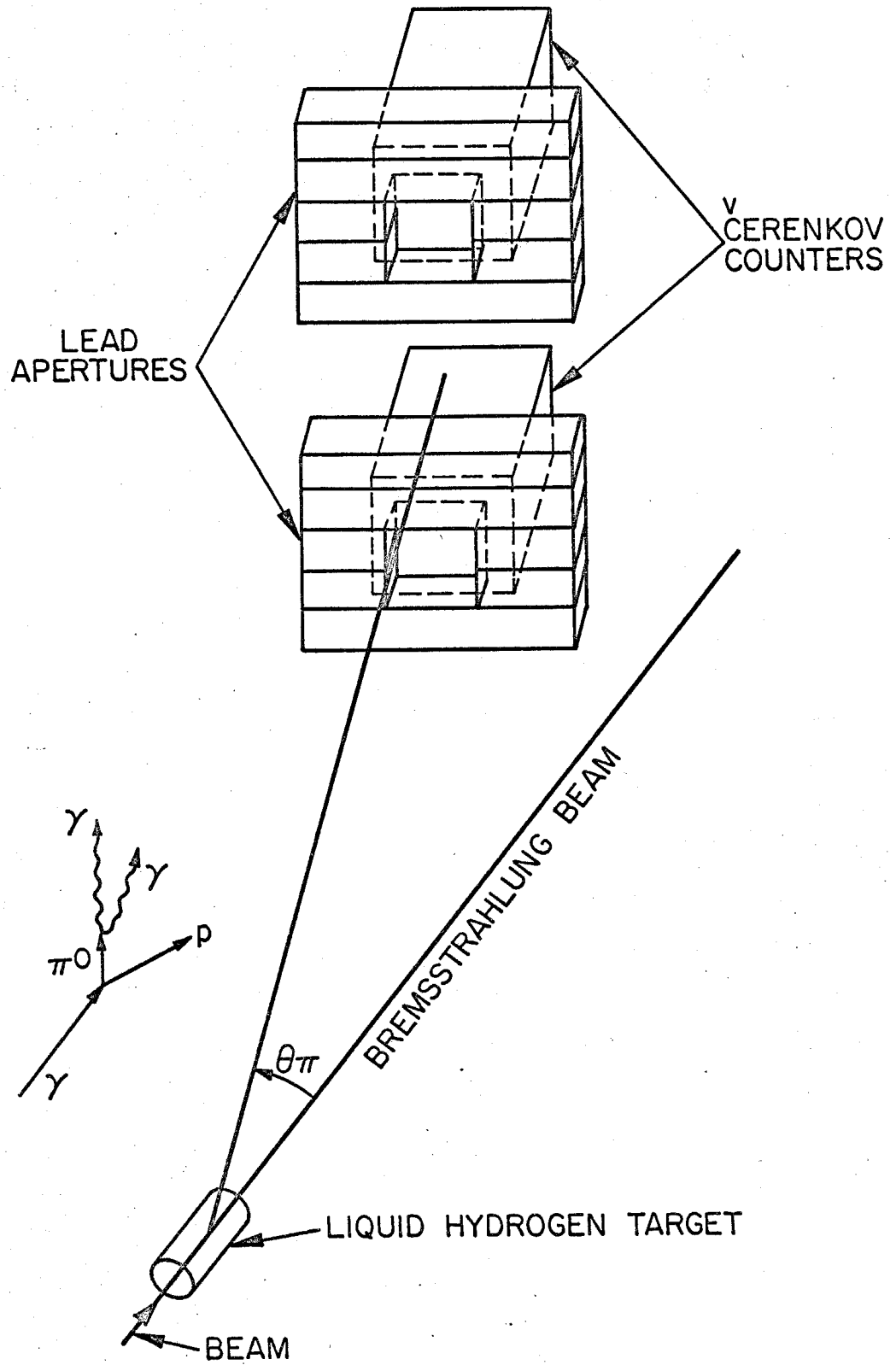

FIGURE 2 EXPERIMENTAL ARRANGEMENT

perpendicular to the beam plane to obtain the desired geometric cutoff energy. The lead houses which surrounded the Cherenkov counters eliminated beam associated particles not passing through the apertures. The apertures themselves were shaped on three sides and backed by a two scintillation counter telescope to veto charged particles. A gamma ray striking the side of the aperture has a high conversion probability so the veto counters accurately define aperture size as well. The sweep magnet was used at small angles to reduce charged particle rates in the veto counters.

The electronics system used is given in Figure 3. A gamma ray is defined by a pulse in the Cherenkov counter with no signal from the aperture charged particle veto counter or from the cosmic ray veto counter. The discriminator also requires the Cherenkov counter pulse to be above a minimum height given by the decay kinematics of detectable pions. A π^0 event is defined by a coincidence between gamma rays in each Cherenkov counter. The pulse heights in each counter then define the X and Y addresses in the 32 x 32 matrix pulse-height analyser.

The energy resolution function is calculated in Appendix IV, and shows the features previously discussed qualitatively. The efficiency for detecting pions produced into the counter rectangle $\epsilon(E_\pi)$ and the number of photons N(k) are given in Figure 4. In order to ignore the scale complication introduced by kinematics, the functions are given at 0 degrees where $E_\pi \cong k$. The total resolution function has the low energy side determined by $\epsilon(E)$ and the high energy side determined by the bremsstrahlung spectrum N(k). The combination of the two gives the spectrum of detected pions $S(k) = N(k) \times \epsilon(k)$. The actual spectrum in pulse height is obtained using the

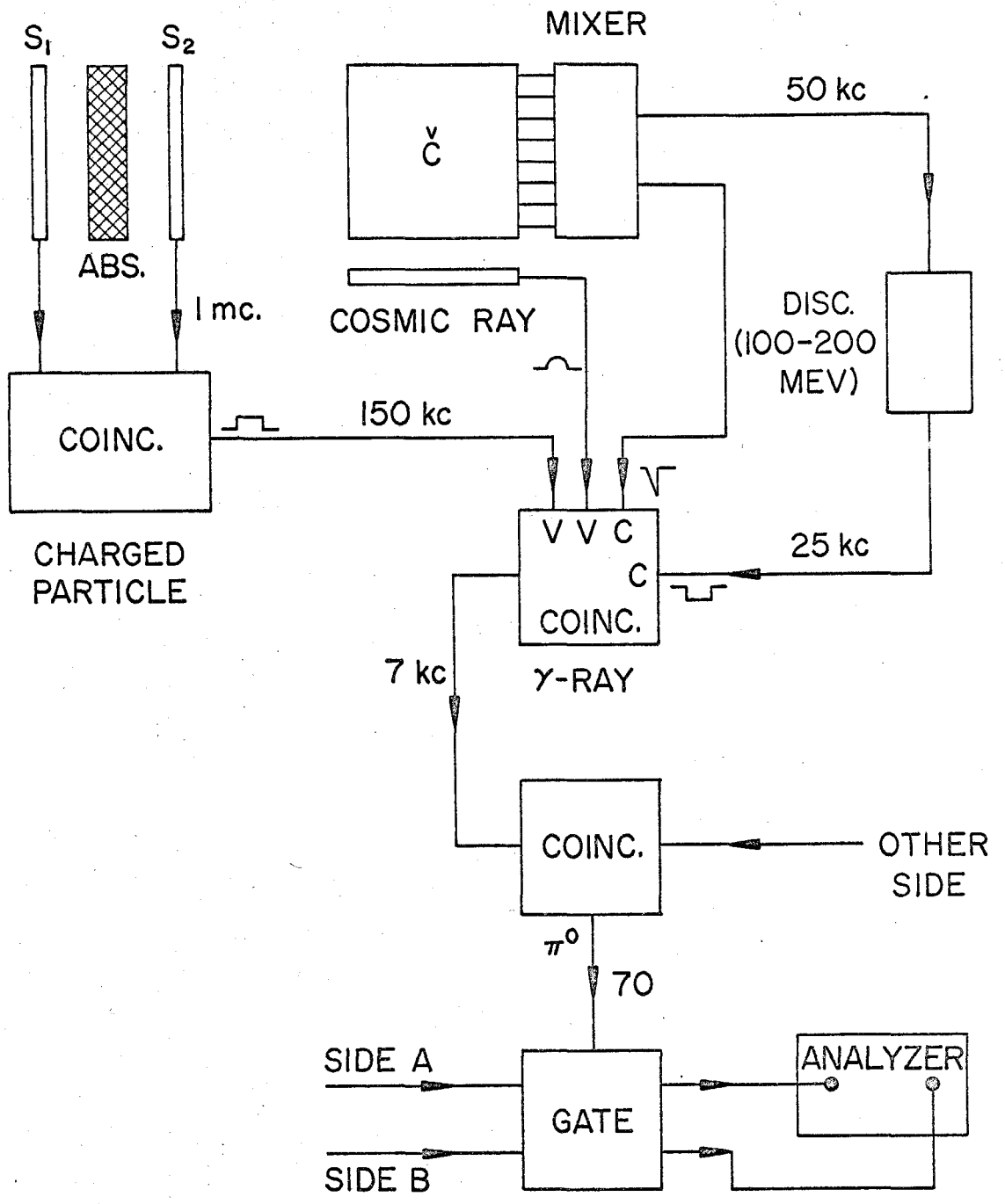

FIGURE 3 ELECTRONIC LOGIC

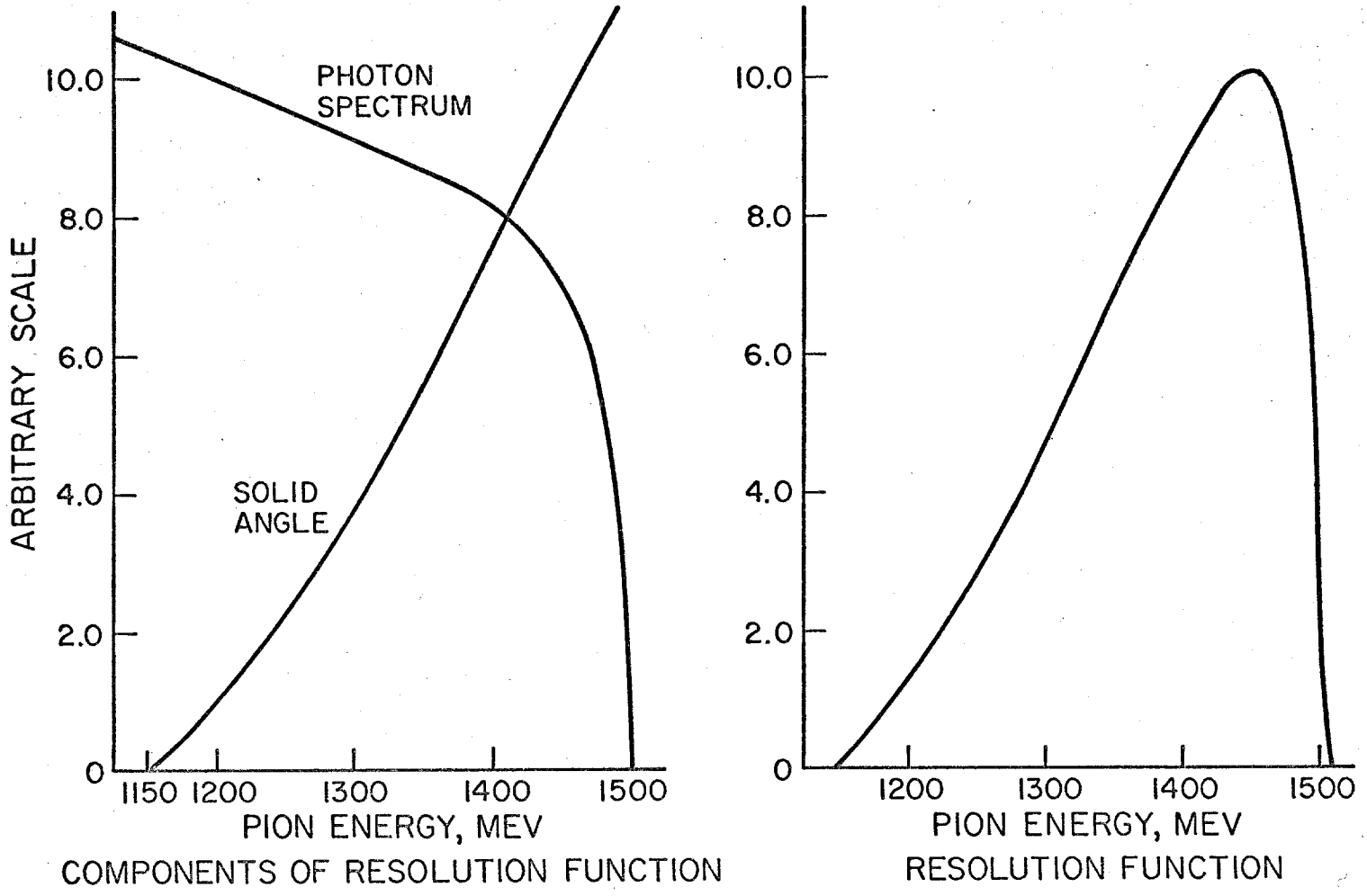

FIGURE 4 CALCULATION OF EXPERIMENTAL RESOLUTION FUNCTION

response function of the counters $R(E, E')$, $S(E_\pi) = \int N(E') \times \epsilon(E') \times R(E_\pi, E')\, dE'$.

The angular resolution in the center of mass for the system is the result of two effects, the physical width of the counter apertures in the laboratory, and the variation in CM angle with energy at constant laboratory angle. These functions are given in Figures 6 and 7.

The actual calculation of the functions takes into account the motion of the nucleons in the deuteron. The results differ from those for a stationary target as follows: 1) for a constant CM cross section the rate of production of pions in the laboratory is increased by less than 2 per cent, 2) the shape of the resolution function in energy as given by its first few moments is not changed by more than 2 per cent, 3) the angular resolution in the center of mass is increased by about 50 per cent.

The choice of running parameters was dictated by the requirement of a reasonable counting rate. Figure 5 shows the system counting rate as a function of cutoff energy. The interval chosen for $E_0 = 1513$ MeV was $E_G = 1150$ MeV. With this choice, the width of the resolution function defined as $\sqrt{\langle (K - \bar{K})^2 \rangle}$ was about 80 MeV. For these limits, $\epsilon(E) = 6 \times 10^{-3}$, so the effective solid angle of the system is about 0.1 millisteradian for an energy acceptance of 160 MeV. The Caltech magnetic spectrometer measuring π^+'s at the same energy has an angular acceptance of 0.1 millisteradians for an energy acceptance of 25 MeV.[5] The rather wide energy acceptance necessary is the principal defect of the system for kinematics definition used here.

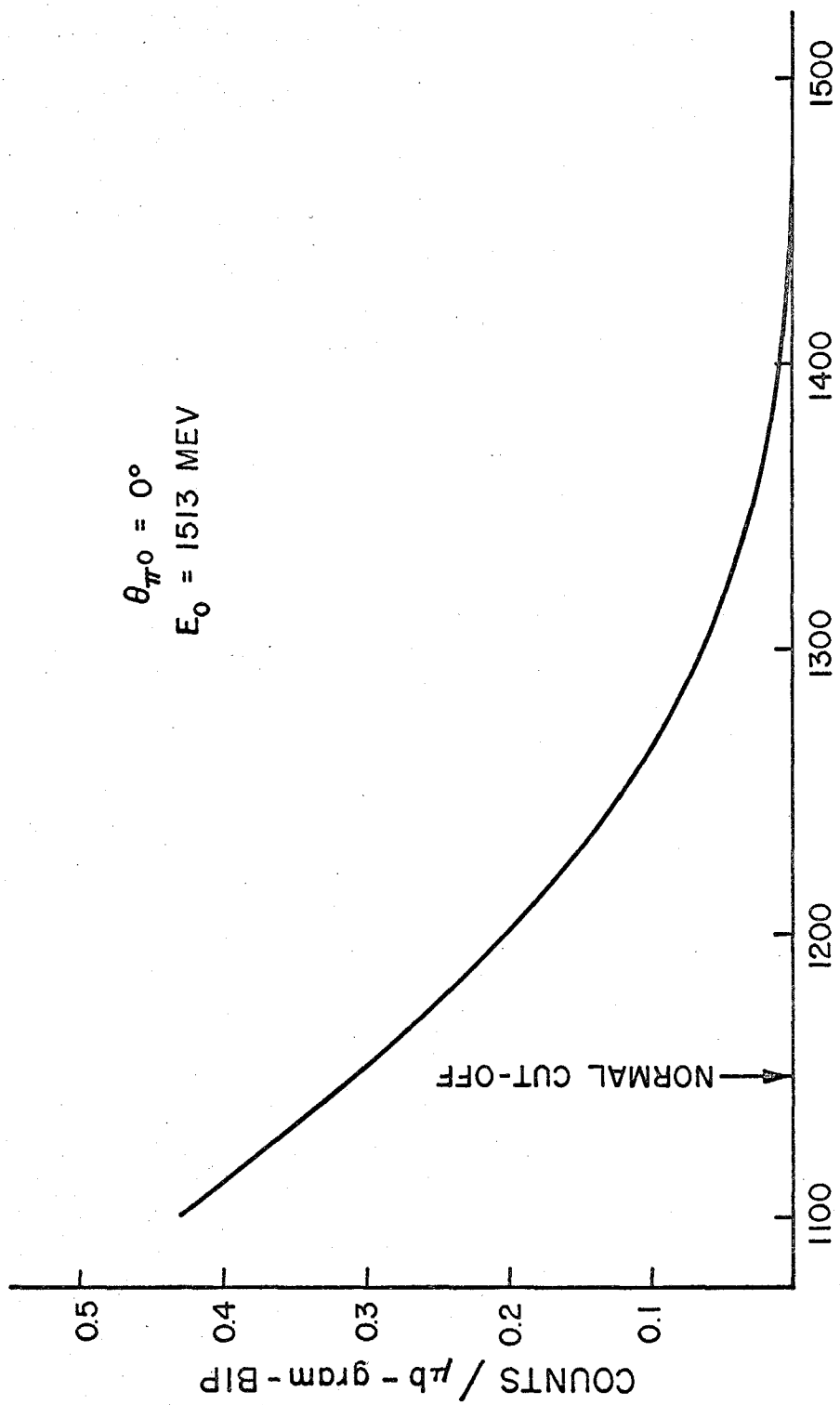

FIGURE 5 COUNTING RATE AS A FUNCTION OF PHOTON CUT-OFF ENERGY

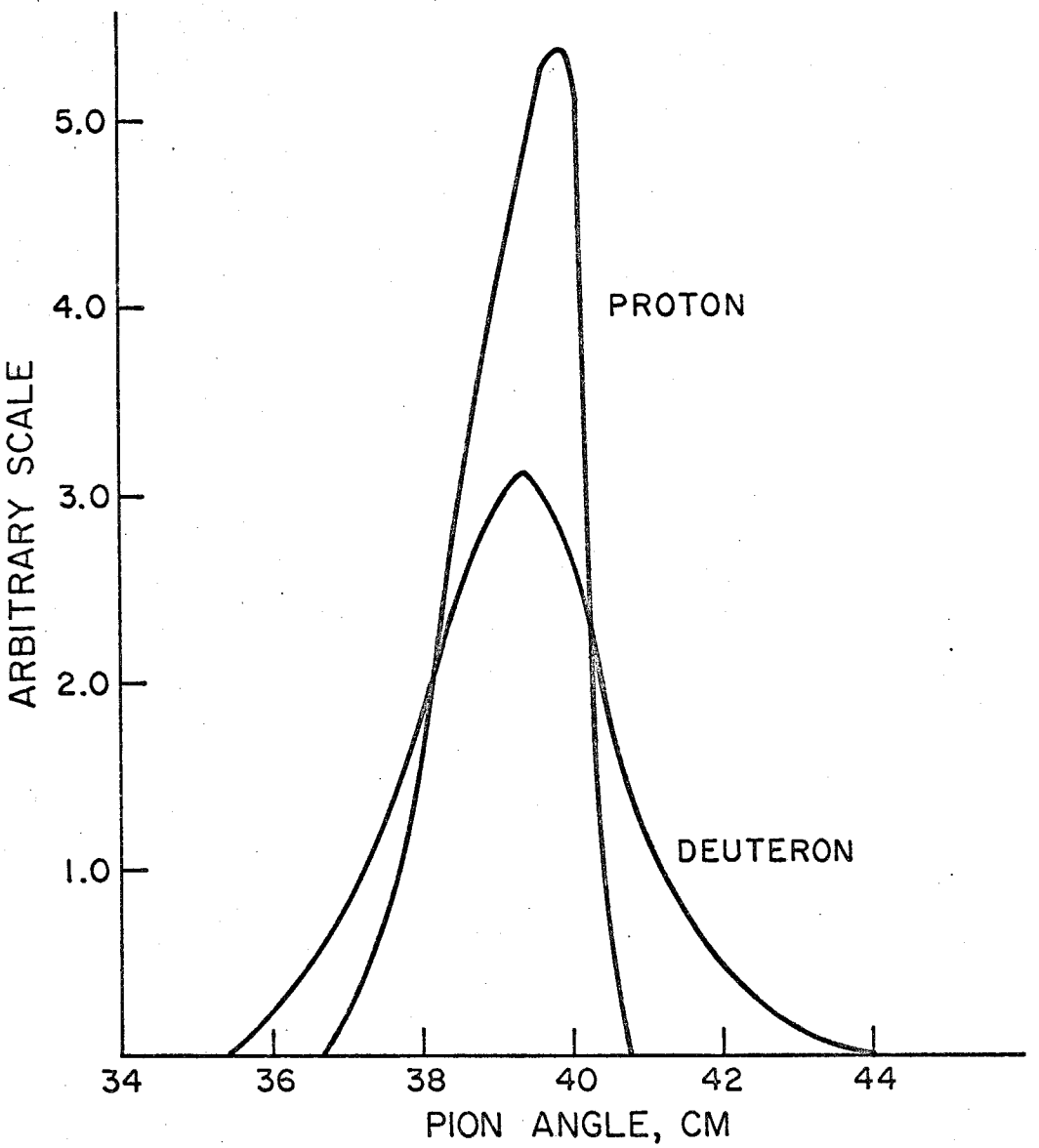

FIGURE 6 ANGULAR RESOLUTION FUNCTION FOR POINT DETECTOR

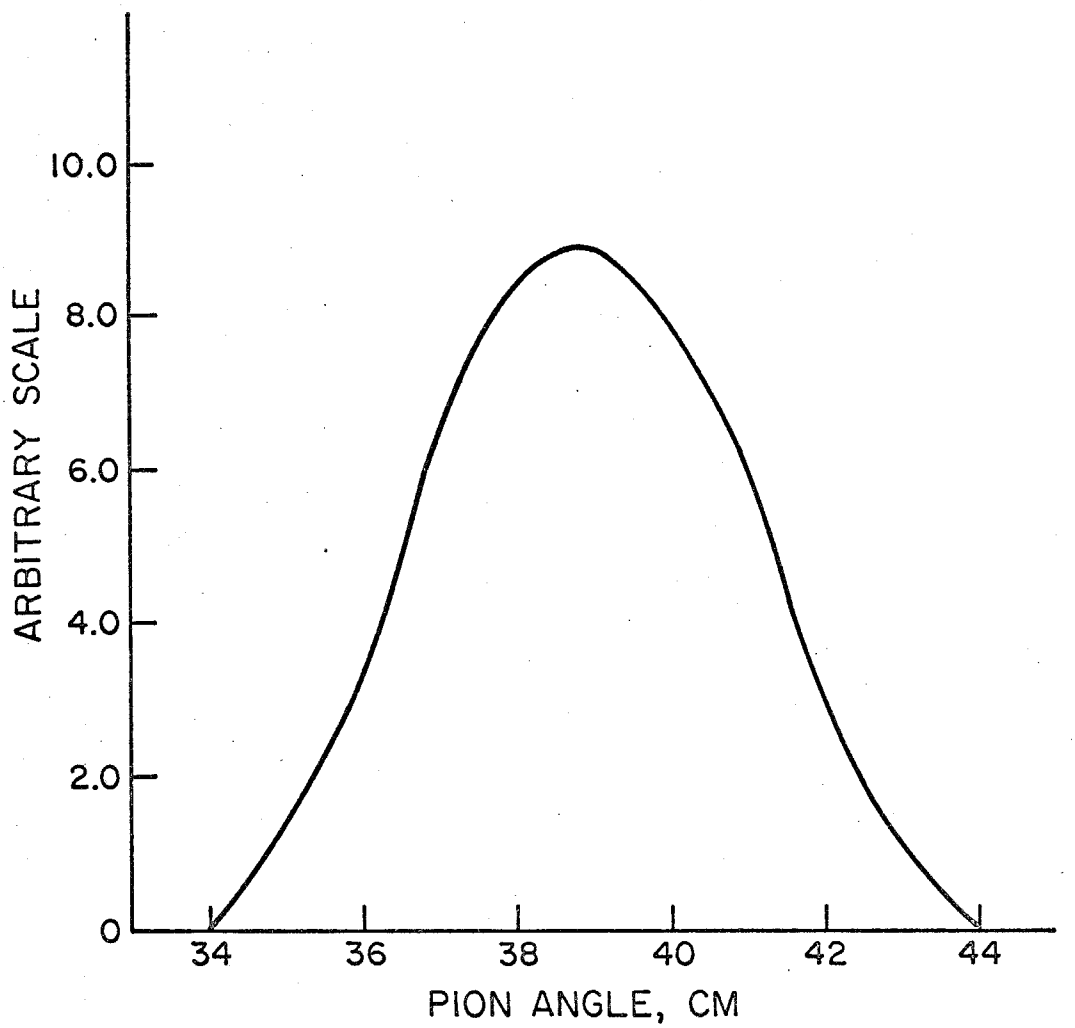

FIGURE 7 EXPERIMENTAL ANGULAR RESOLUTION FUNCTION

III. PROCEDURE

The experiment was run over an 18 month period at three endpoint energies, E_o = 1073, 1308, and 1513 MeV. The angular distributions were taken at 10 degree intervals in the center of mass from 0 degrees to 90 degrees. The distributions required several different configurations, with each point within a given configuration taken several times. The details of configuration and consistency checks between configurations are given in Appendix II. The target condensed either hydrogen or deuterium with the same apparatus. The hydrogen and deuterium runs were taken alternately, providing a hydrogen-deuterium ratio free of most of the systematic errors.

The background runs were taken throughout the running period, usually on the same day as the foreground. The 911 and 1182 MeV data show no statistically significant time variation in background rate for points taken in the same configuration. Some of the 1390 MeV data were taken with rather poor beam definition due to instabilities inherent in the synchrotron beam when running at an endpoint of 1513 MeV. For these runs it was necessary to compare the foreground runs with the background runs taken on the same day, although in these cases the difference in the foreground rates was less than 20 per cent.

The phototube gain was monitored by measurement of the pulse-height spectrum from the Cherenkov counters on cosmic ray muons. The measurement was done each day during the 12 hours while the experiment was not run. The mean pulse height was determined by comparison with the mono-energetic electron beam to

TABLE 1

Run Parameters

Distribution	Endpoint Energy, MeV	Cutoff Energy, MeV	Mean Photon Energy, MeV	Full Width 1/2 Max, MeV	Angles Covered
1.	1065	700	920	200	0^{o} - 80^{o}
2.	1308	950	1175	218	0^{o} - 90^{o}
3.	1510	1150	1375	186	0^{o} - 90^{o}

correspond to 220 MeV electrons. The electronic gain was not a linear function of pulse height, but was measured daily by means of a simulated Cherenkov pulse produced by a pulser with a linear scale. The known linearity of the counters and these two measurements give daily energy calibration of the system.

The rates encountered in the beam area are given in Table 2 for the various points in the system for the E_o = 1308 MeV data from hydrogen. The counts were about 2/3 from deuterium, 1/3 from background. The hydrogen rates were about 0.8 times these. There are four electronic problems to consider:

1) accidentally vetoed gamma rays,

2) charged particles not vetoed due to dead time in the veto discriminator,

3) coincident gamma-ray events not recorded due to dead time in the analyser, and

4) accidental coincidences between the two Cherenkov counters.

1) and 2) arise from high rates in the aperture veto telescope. The counting rate in a single scintillation counter is principally due to Compton electrons produced by the halo of low energy photons which fill the beam area. The use of a two counter telescope eliminates these electrons setting a low energy bias of about 15 MeV. The single counter rate is about 8 times the coincidence rate. The resulting rate keeps 1) and 2) less than 0.5% by measurement. The analyser had a 5 kilocycle acceptance rate so 3) is negligible.

TABLE 2

Counting Rates

E_o = 1308 MeV

f = deuterium runs

b = empty target runs

Angle, Lab		Rate, Counts/Second Veto Scint. $\times 10^3$	Veto Coinc. $\times 10^3$	Gamma >100 MeV $\times 10^3$	Electrons >100 MeV $\times 10^3$	Pions
0^o	f	1060	110	10.0	3.0	7.3
	b	540	40	5.3	0.5	4.0
20^o Mag On	f	240	34	4.8	12.0	2.9
	b	120	19	1.6	10.0	0.3
20^o Mag Off	f	1200	340	3.0	2.8	1.7
	b	600	170	1.7	0.45	0.5
42^o	f	420	65	2.6	0.8	0.8
	b	300	50	0.2	0.1	0.1

The rate of accidental coincidences between the two Cherenkov counters is not negligible at some points and required constant monitoring at all times. The rate $(\gamma_A + 100\ \text{ns}) \cdot (\gamma_B)$ was monitored by a separate circuit. Each foreground run at which the rate made a correction necessary was followed by an accidental π run, delaying the γ_A pulse through the normal π coincidence circuit. The synchrotron intensity was kept at values such that the accidental coincidence rate did not exceed 10% of the foreground rate, and was usually less than 5% of the foreground rate.

The 32×32 pulse-height matrix contained in the analyser was written onto paper tape for preliminary analysis by the Burroughs 220, and ultimately converted to IBM cards for the final analysis using the pulse height to energy calibration.

IV. DATA REDUCTION

The system has produced a 32 x 32 matrix in pulse height of coincident gamma-ray pairs for each foreground, background and accidental run. The Cherenkov counter and electronic gain calibrations are used to generate a matrix in energy from the matrix in pulse height. The scale of these matrices is then converted to one linear in energy. The process of conversion and its associated errors is given in Appendix II. The resulting background and accidental matrices can now be subtracted from the corresponding foreground matrices to obtain the result from hydrogen or deuterium. The result next obtained from this matrix is the spectrum in total energy of the detected two gamma-ray events. This spectrum is given by the sum of the matrix diagonals,

$$S(E) = \int_0^E M(E - E_{\gamma 2}, E_{\gamma 2})\, dE_{\gamma 2} \quad .$$

The reactions which produce a significant number of events are:

1) the reaction of interest $\gamma + d \rightarrow \pi^o + (p + n)$

2) single π^o's from double π production,
$\gamma + d \rightarrow \pi^o + (\pi + N + N')$

3) events resulting from the detection of one gamma ray from each π^o in $\gamma + d \rightarrow \pi^o + \pi^o + (p + n)$.

The desired reaction, 1), will contribute to the spectrum above the geometric cutoff energy. The detection of reaction 2) is a by-product of the large pion energy acceptance, which places the geometric cutoff energy well below the maximum pion energy in two pion production. Since a single π^0 is detected, reaction 2) only contributes events with total energies greater than the cutoff. For a given total cross section, the counting rate and the energy spectrum from these pions is calculated in Appendix V from two models, 1) pure phase space, and 2) resonant production by the reaction $\gamma + N \rightarrow \pi^0 + N^*(1238\ \text{MeV})$. An upper limit for this reaction has also been obtained at one point by means of the synchrotron subtraction technique. The results for two pion contamination are given below:

1) phase space with a total cross section of 200 μbarns, which is 5 times the value measured for $\gamma + p \rightarrow \pi^+ + \pi^- + p$[6] gives a correction of less than 5 per cent,

2) production of a π^0 and N*(1238 MeV) with a total cross section of 200 μbarns[7] gives a correction of 10 per cent at 0°, falling to 4 per cent at 50°,

3) the synchrotron subtraction at 40°, $k_{av} = 1182$ MeV, gives a correction of 3 ± 3 per cent,

4) fitting of the computed spectrum to the observed spectrum shows no statistically significant enhancement of the low energy cross section. This procedure puts an upper limit of about 0.05 μbarn on the cross section due to multiple pions, or an upper limit of 20 per cent

at 0^{o}, falling to 4 per cent at 40^{o}.

Since it is not possible to make an angle dependent correction, no change has been made to the quoted cross sections. As such, they are the sum of all reactions $\gamma + N \rightarrow \pi^{o} + N'$ producing single π^{o}'s into the given resolution function.

The energy distribution of detected gamma-ray pairs in 3) can be understood qualitatively. Unlike single π^{o} detection, there is no lower limit from the system geometry on the total energy of the two detected gamma rays, so the energy spectrum of these events extends from zero to its maximum. Furthermore, any photon of energy above the two pion threshold can produce events, so the spectrum will contain a large number of low energy counts. In the actual experiment a lower limit of about 100 MeV is given to the energy of each gamma ray by the bias set on the Cherenkov pulse into the coincidence circuit which defines a gamma-ray event. The maximum total energy can be understood as follows. The kinematics for producing a two pion system of mass $2m_{\pi}$ is very little different from that of a single pion at the same angle, or $E_{\pi 1} + E_{\pi 2} = E_{\pi}$. A foreward going gamma ray carries almost all of the energy of the π^{o}, e. g., at $E_{\pi} = 500$ MeV, $E_{\gamma}(\max) = 495$ MeV. Hence reaction 3) can provide events with total energy almost up to that of single pion photoproduction. The contribution of the third reaction above the single π^{o} detection cutoff requires a correction of about 10 per cent at 0^{o} and 10^{o} and is negligible at large angles. The details of the method of estimating the correction from the data are given in Appendix II.

The energy spectrum from each of these reactions is given in Figure 8. The pulse-height spectrum obtained by the data reduction is given in Figure 9. This spectrum shows a good separation between the single and double π^0 regions, making it a simple matter to determine the counting rate by counting π^0's above the cutoff. The more sophisticated procedure of using fitting functions for the two regions, together with the errors due to double π^0 detection, is given in Appendix II. Finally, a spectrum with an excellent separation of single π^0's is compared with the computed spectrum in Figure 10.

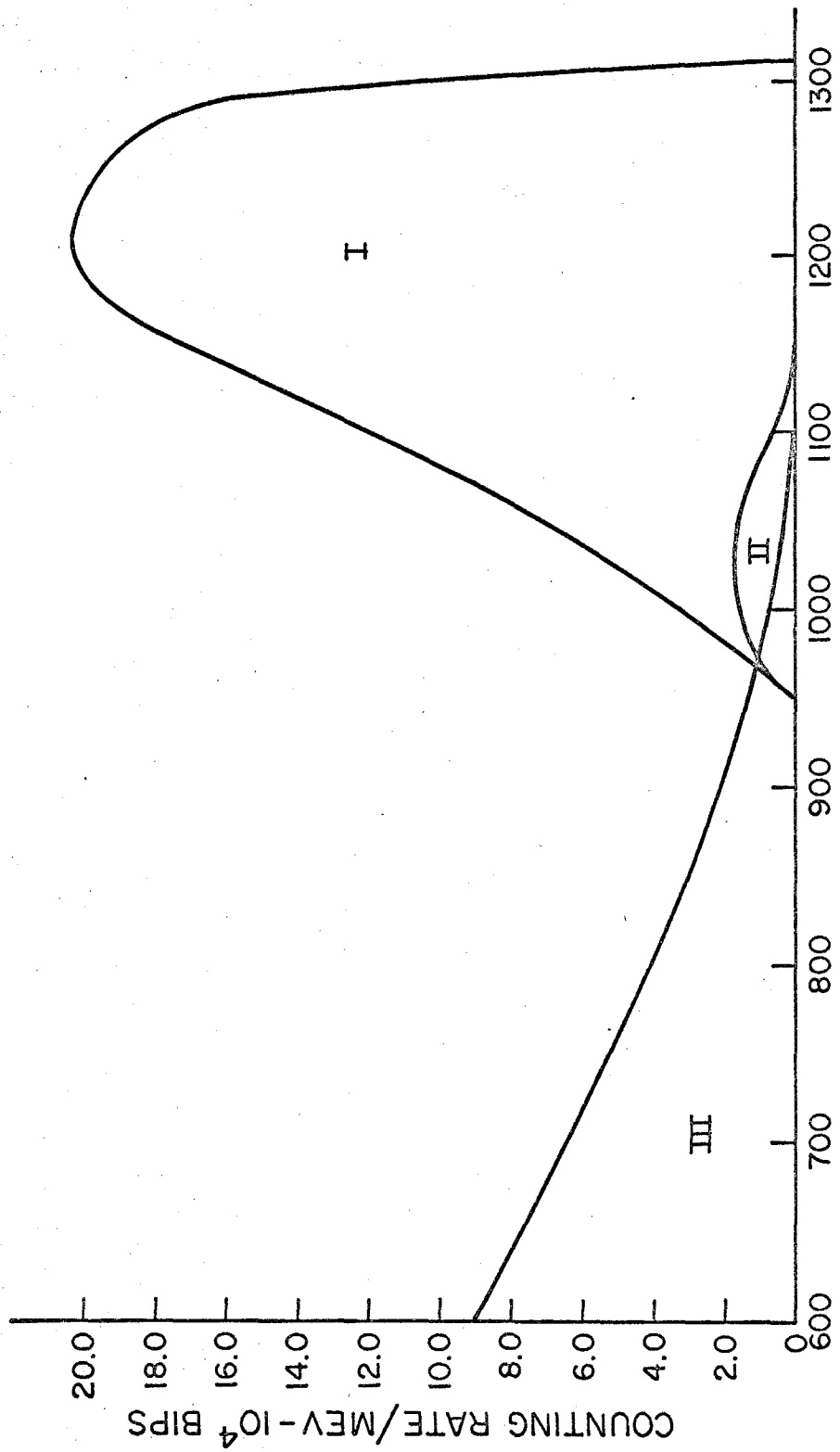

FIGURE 8 ENERGY DISTRIBUTION OF COINCIDENT GAMMA RAYS

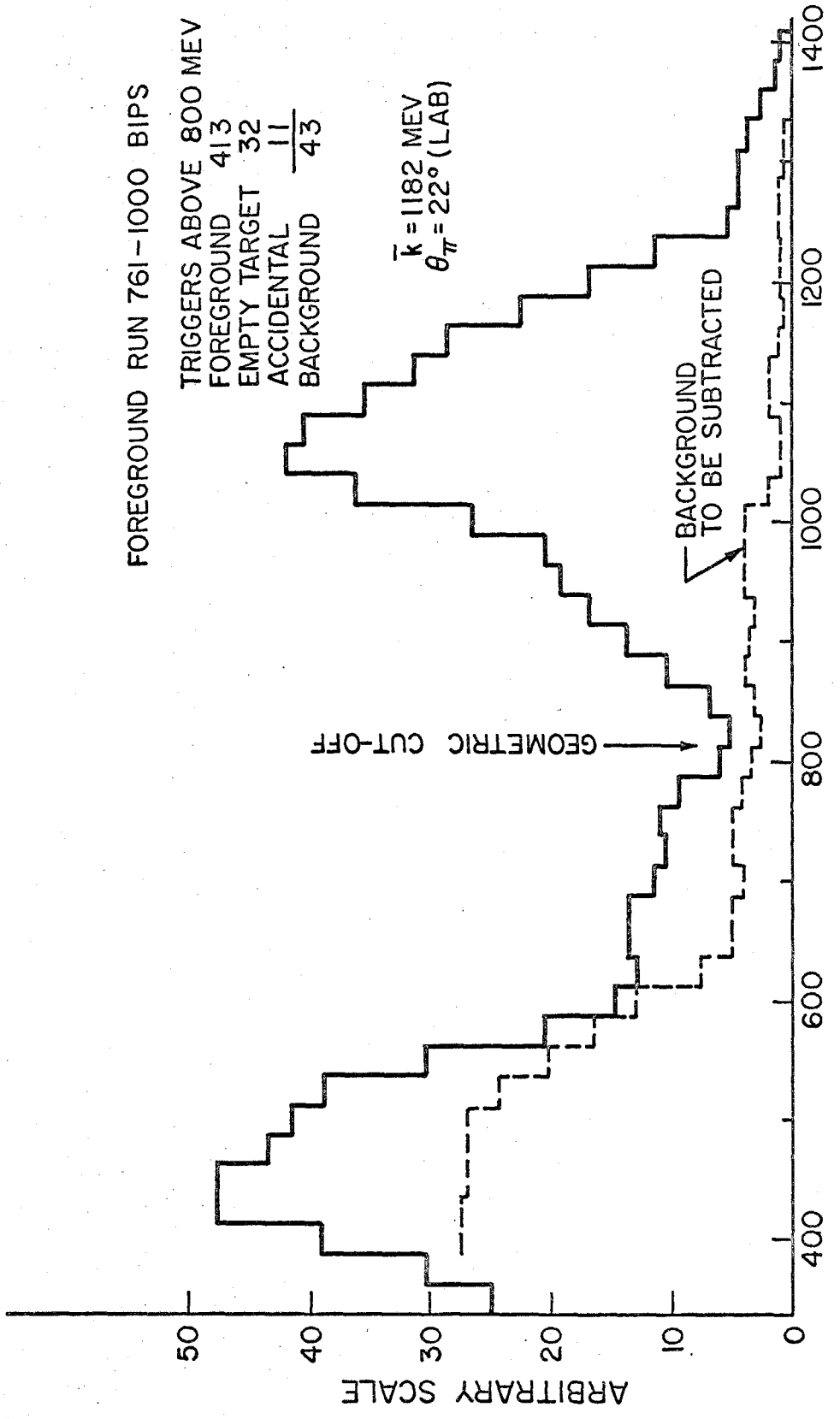

FIGURE 9 SUM SPECTRUM FROM RECALIBRATED MATRIX

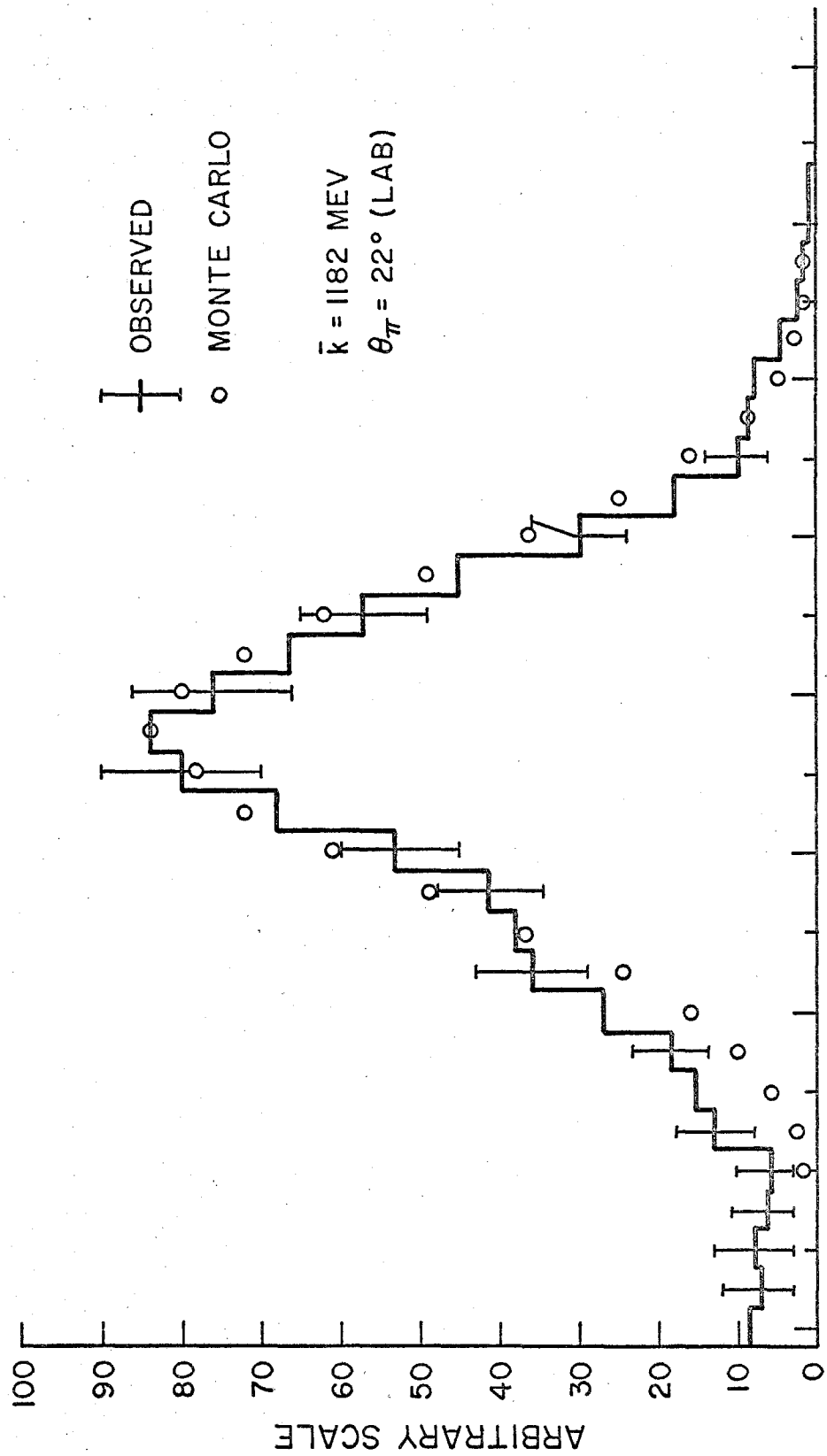

FIGURE 10 OBSERVED AND COMPUTED ENERGY SPECTRUM FOR DETECTION OF SINGLE PIONS

V. CROSS SECTIONS

The results of the experiment are given in the tables which follow as the three directly measured quantities, the proton and deuteron cross section, and the deuteron/proton ratio. The proton cross sections have been taken from Reference 3. We have also given the result for a "neutron" cross section assuming the simplest spectator model, for which the deuteron cross section is simply the sum of the free proton and neutron cross sections, $\sigma_d = \sigma_p + \sigma_n$.

The cross sections quoted are obtained from the counting rate at each point by the equation $C = \eta \times \bar{\sigma}(k_o, \theta_o)$ where η is the integral of the geometric resolution function at that point, as described in Appendix III. Summarizing the results obtained there, where $T(k, \theta)$ is the resolution function,

$$C = \int \sigma(k, \theta)\, T(k, \theta)\, dk d\theta$$

$$\simeq \eta \times \left\{ \sigma(k_o, \theta_o) + \frac{\partial^2 \sigma}{\partial k^2}\bigg|_{k_o \theta_o} \langle (k - k_o)^2 \rangle \right\} .$$

The size of $\partial^2\sigma/\partial k^2$ is estimated from the energy distribution data at 60^o and 90^o. The correction is apparently less than 5%. No attempt has been made to correct the data. The statistical errors are:

1) counting statistics on foreground, background and accidental runs,

2) calibration error, leading to incorrect combination of runs,

3) subtraction of the $(\pi^o\pi^o)$ spectrum,

4) setting of the geometrical parameters.

Systematic errors may be defined by $\bar{\sigma}(k,\theta) = \sigma(k_o,\theta_o) \times \{1+\delta(k,\theta)\}$. The sources of error and typical values are:

1) detection of single π^o's in double π production, $-.05 \leq \delta(k,\theta) \leq 0$,

2) deviation from the true value due to energy variation of cross section, $|\delta(k,\theta)| < 0.05$,

3) endpoint energy of synchrotron, $|\delta| < .03\ \text{MeV}^{-1}$ (This correction is independent of angle to about 5%),

4) absolute normalization of beam monitoring, $|\delta| < 0.02$ (This correction is time dependent, since the quantameter calibration may change.),

5) calculation of detection efficiency, including the small corrections, $|\delta| < 0.02$.

TABLE 3a

Cross Section Data

$\bar{k}$ = 911 MeV

Angle, CM	Deuteron Cross Section, μbarns/steradian	Deuteron/Proton Ratio
3.5	1.406 ± 0.132	3.161 ± 0.394
11.2	1.831 ± 0.124	3.237 ± 0.407
20.3	2.688 ± 0.127	3.841 ± 0.462
28.0	3.056 ± 0.105	2.093 ± 0.165
38.1	3.080 ± 0.125	1.921 ± 0.126
47.9	3.001 ± 0.108	1.842 ± 0.096
57.4	2.833 ± 0.119	1.688 ± 0.098
67.3	3.218 ± 0.129	1.642 ± 0.096
77.5	3.591 ± 0.197	1.660 ± 0.122

TABLE 3b

Cross Section Data

$\bar{k}$ = 1182 MeV

Angle, CM	Deuteron Cross Section, μbarns/steradian	Deuteron/Proton Ratio
3.7	0.728 ± 0.049	1.584 ± 0.183
11.4	1.295 ± 0.161	2.162 ± 0.350
21.4	2.591 ± 0.122	2.334 ± 0.164
31.9	2.881 ± 0.206	2.036 ± 0.164
41.8	2.812 ± 0.214	1.806 ± 0.153
51.6	2.045 ± 0.078	1.501 ± 0.094
61.6	1.602 ± 0.119	1.291 ± 0.120
72.0	1.651 ± 0.106	1.602 ± 0.145
81.6	1.338 ± 0.099	1.541 ± 0.158
91.0	1.445 ± 0.133	1.635 ± 0.190

TABLE 3c

Cross Section Data

$\bar{k}$ = 1390 MeV

Angle, CM	Deuteron Cross Section, μbarns/steradian	Deuteron/Proton Ratio
3.1	1.155 ± 0.159	1.858 ± 0.401
10.5	2.408 ± 0.246	1.937 ± 0.387
19.6	2.661 ± 0.213	2.192 ± 0.254
29.6	3.017 ± 0.191	1.820 ± 0.175
39.2	2.166 ± 0.118	1.597 ± 0.140
49.6	1.608 ± 0.097	2.000 ± 0.229
60.3	1.000 ± 0.121	1.688 ± 0.333
70.2	0.898 ± 0.132	1.681 ± 0.356
80.8	1.180 ± 0.164	1.202 ± 0.224
90.7	1.244 ± 0.221	1.264 ± 0.310

TABLE 4a

Difference of Deuteron and Proton Cross Sections

$\bar{k}$ = 911 MeV

Angle, CM	Cross Section μbarns/steradian		Error
3.5	0.961	±	0.175
11.2	1.265	±	0.230
20.3	1.988	±	0.323
28.0	1.596	±	0.240
38.1	1.477	±	0.202
47.9	1.372	±	0.156
57.4	1.155	±	0.164
67.3	1.258	±	0.188
77.5	1.427	±	0.264

TABLE 4b

Difference of Deuteron and Proton Cross Sections

$\bar{k}$ = 1182 MeV

Angle, CM	Cross Section μbarns/steradian		Error
3.7	0.268	±	0.084
11.4	0.096	±	0.210
21.4	1.480	±	0.182
31.9	1.466	±	0.233
41.8	1.255	±	0.238
51.6	0.683	±	0.127
61.6	0.361	±	0.149
72.0	0.620	±	0.150
81.6	0.470	±	0.137
91.0	0.561	±	0.168

TABLE 4c

Difference of Deuteron and Proton Cross Sections

$\bar{k}$ = 1390 MeV

Angle, CM	Cross Section μbarns/steradian		Error
3.1	0.533	±	0.249
10.5	1.164	±	0.480
19.6	1.447	±	0.309
29.6	1.359	±	0.291
39.2	0.810	±	0.190
49.6	0.804	±	0.184
60.3	0.408	±	0.197
70.2	0.364	±	0.190
80.8	0.199	±	0.220
90.7	0.260	±	0.306

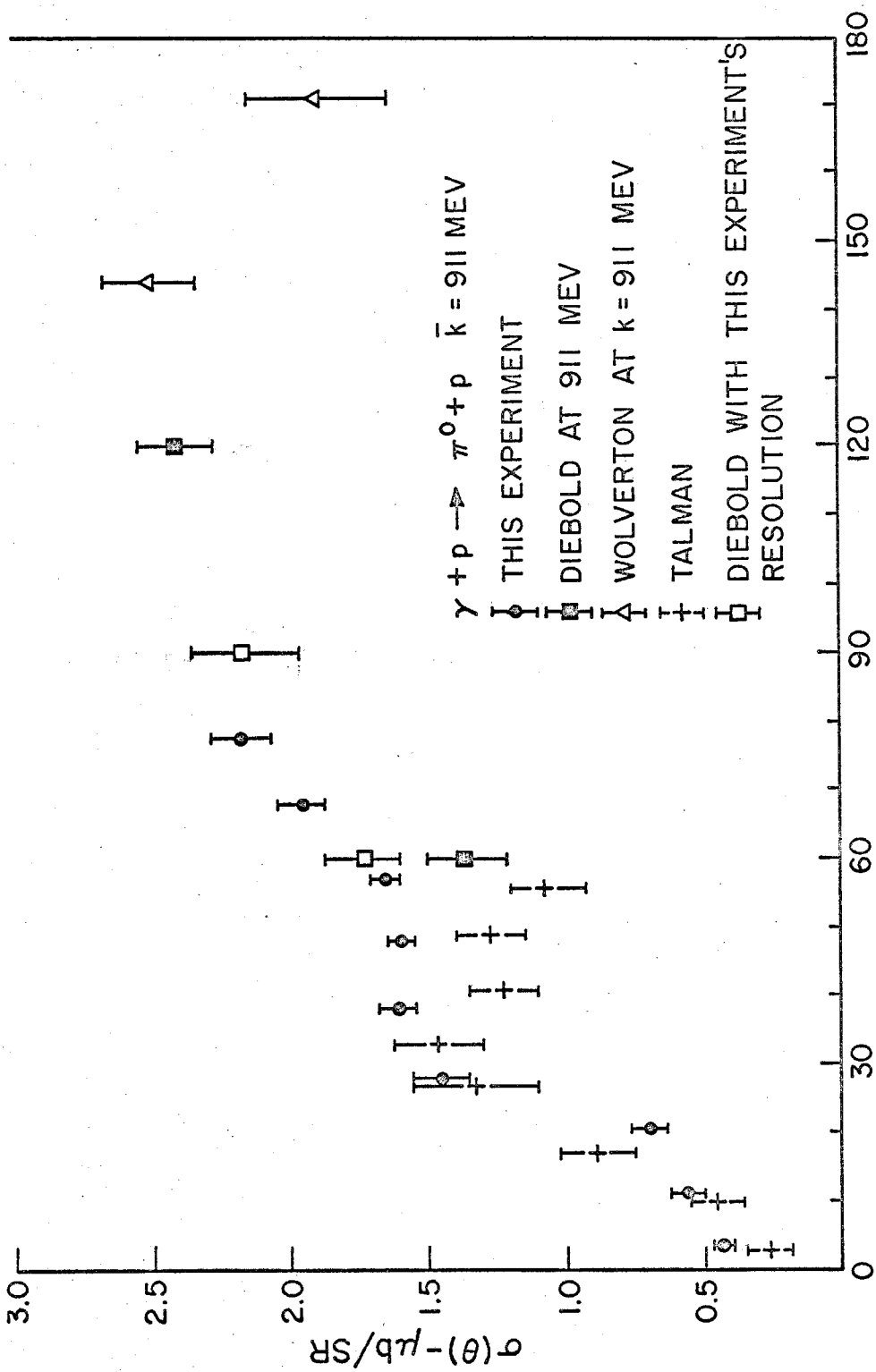

FIGURE IIa π^0 PHOTOPRODUCTION CROSS-SECTION $\gamma + p \rightarrow \pi^0 + p$ NEAR $\bar{k} = 911$ MEV

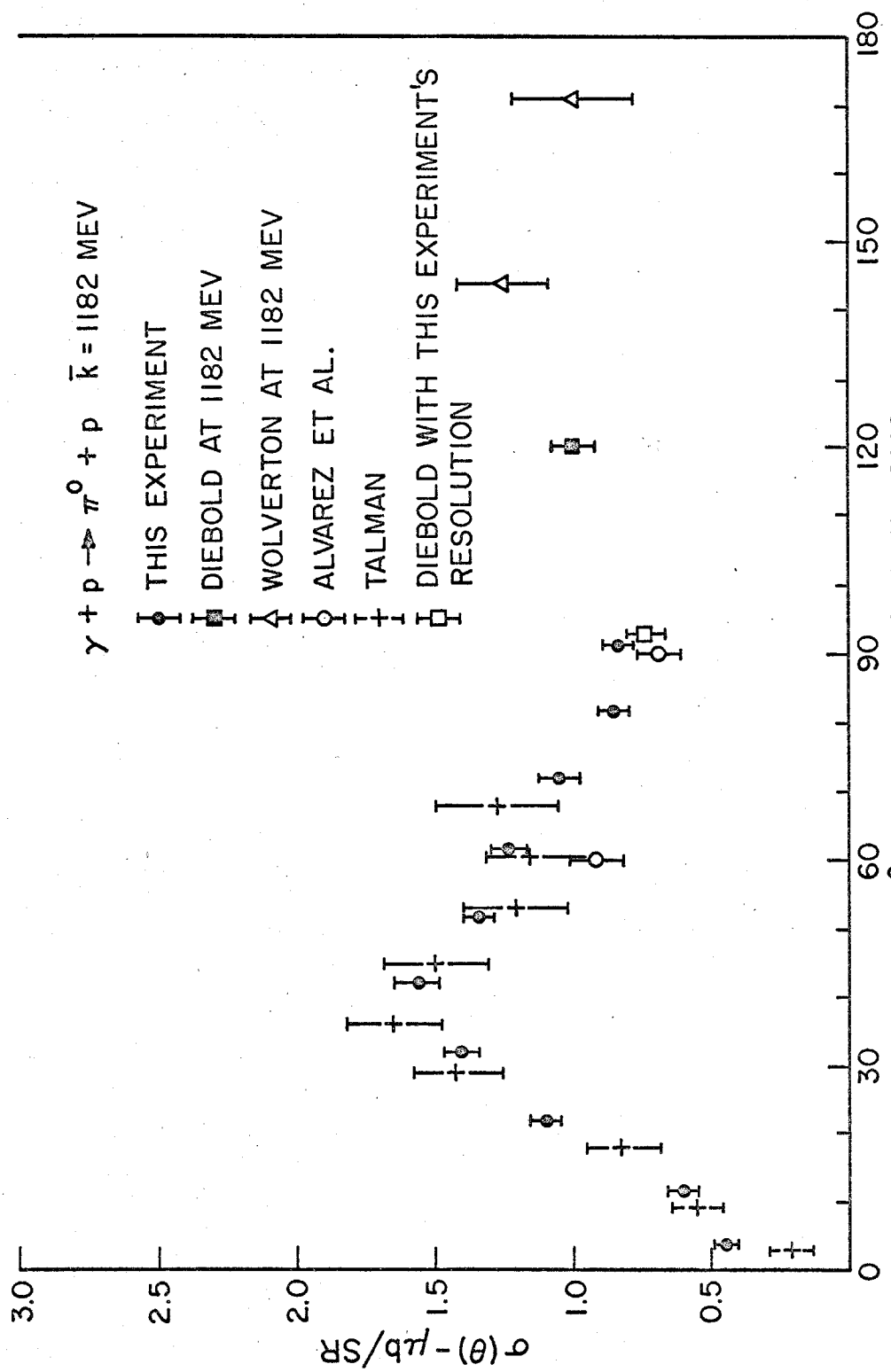

FIGURE IIb π^0 PHOTOPRODUCTION CROSS-SECTION $\gamma + p \rightarrow \pi^0 + p$ NEAR $\bar{k} = 1182$ MEV

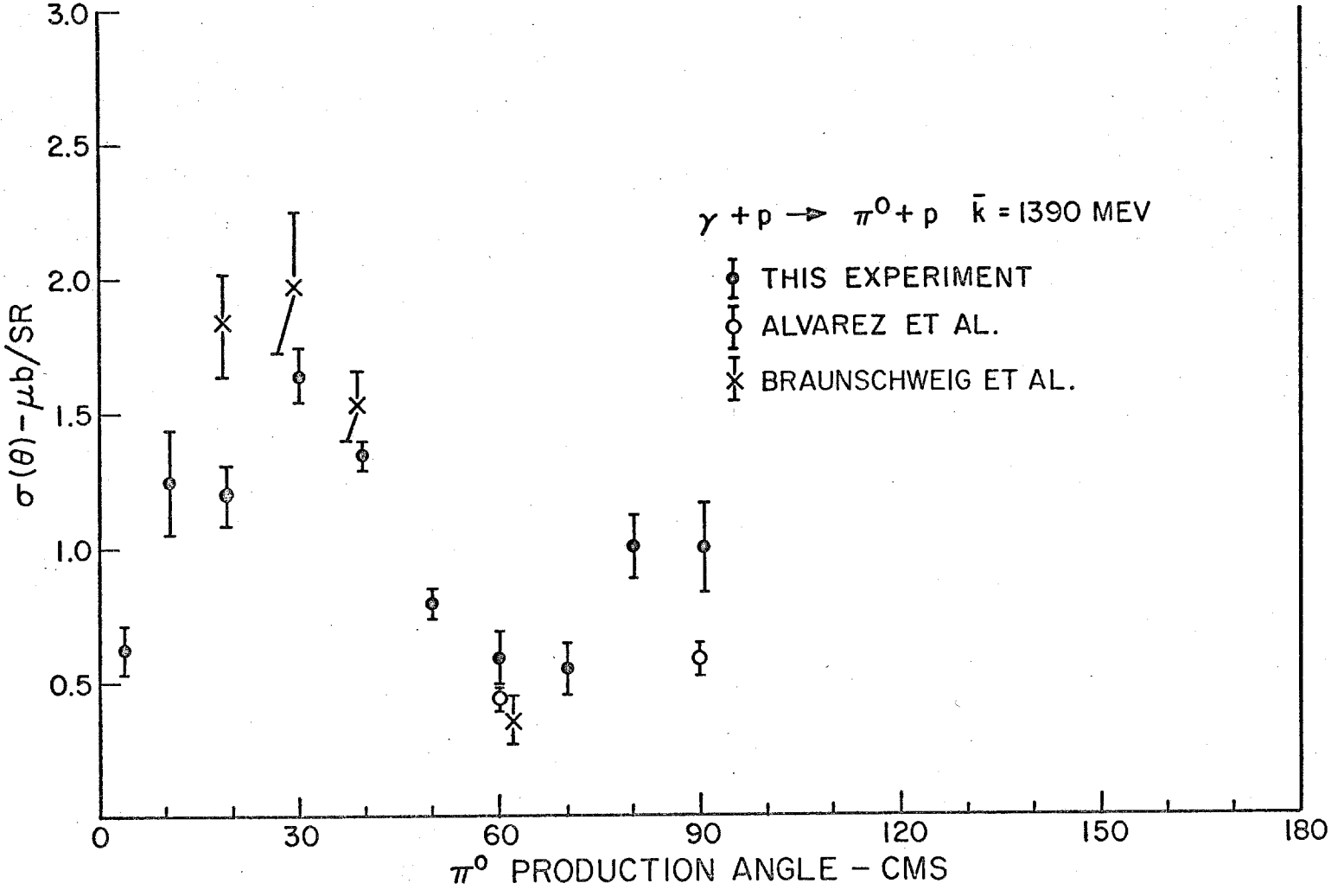

FIGURE IIc π^0 PHOTOPRODUCTION CROSS-SECTION $\gamma + p \rightarrow \pi^0 + p$ NEAR $\bar{k} = 1390$ MEV

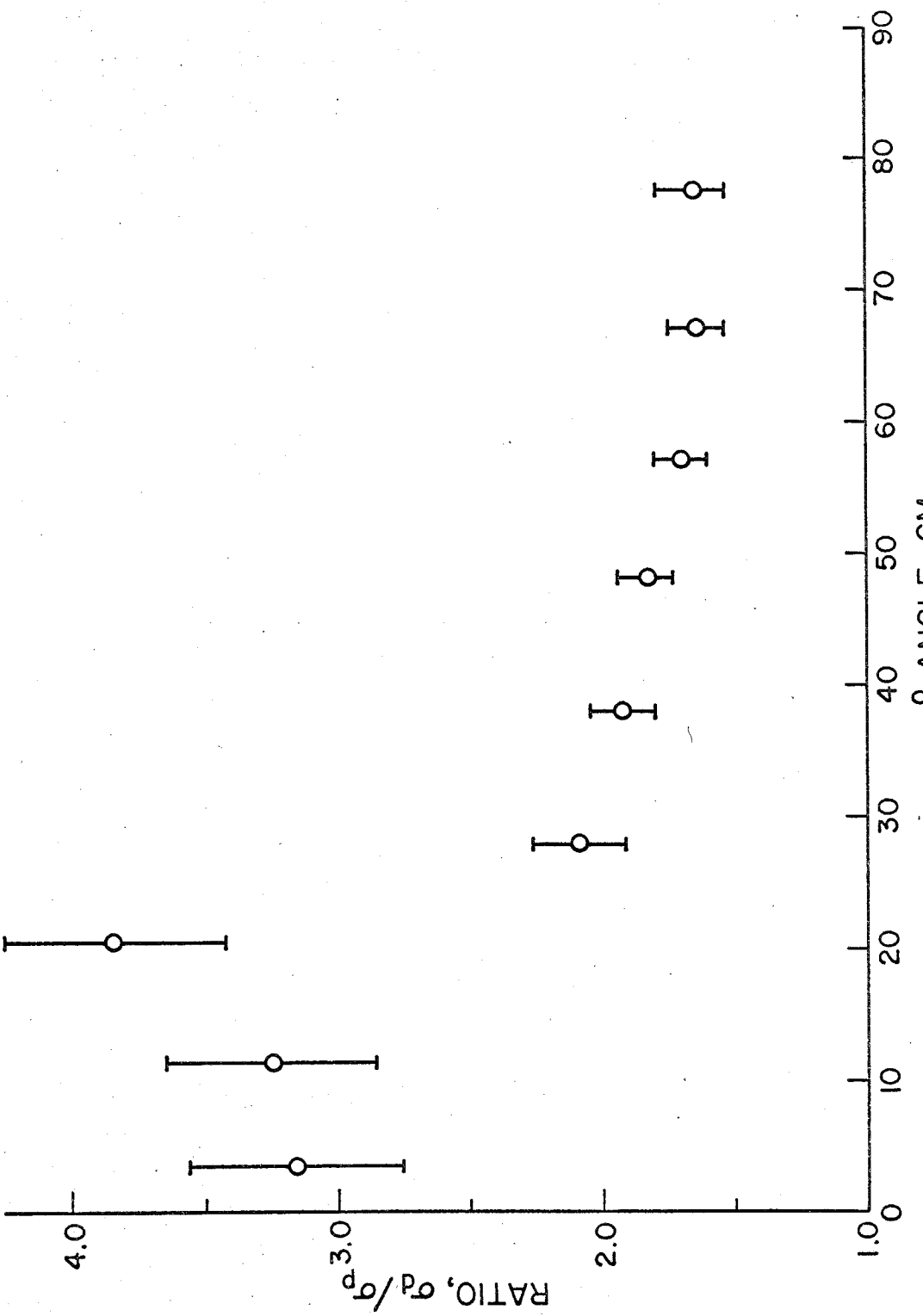

FIGURE 12a DEUTERON-PROTON CROSS SECTION RATIO, $\bar{K}$ = 911 MEV

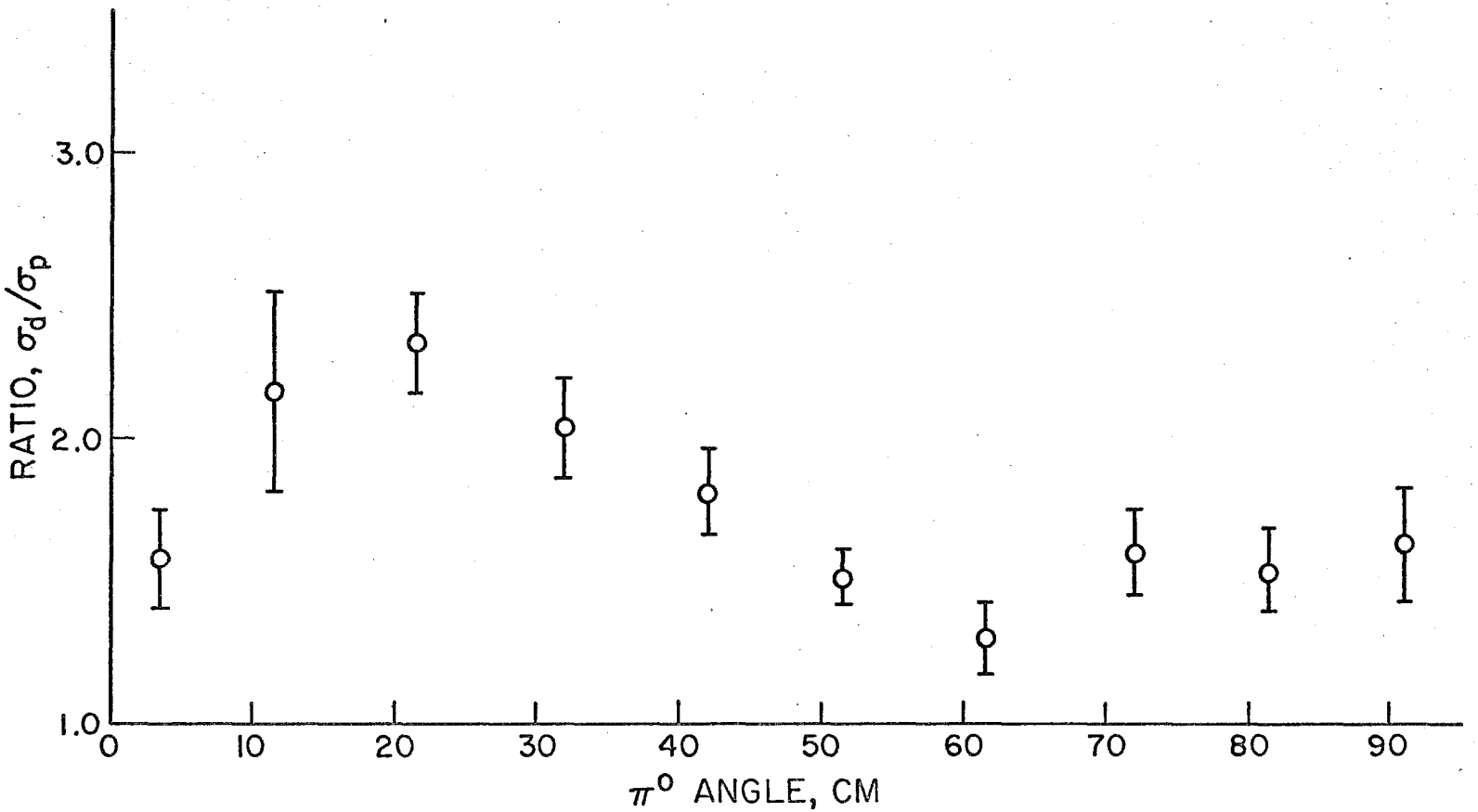

FIGURE 12 b DEUTERON-PROTON CROSS SECTION RATIO, $\bar{K}$ = 1182 MEV

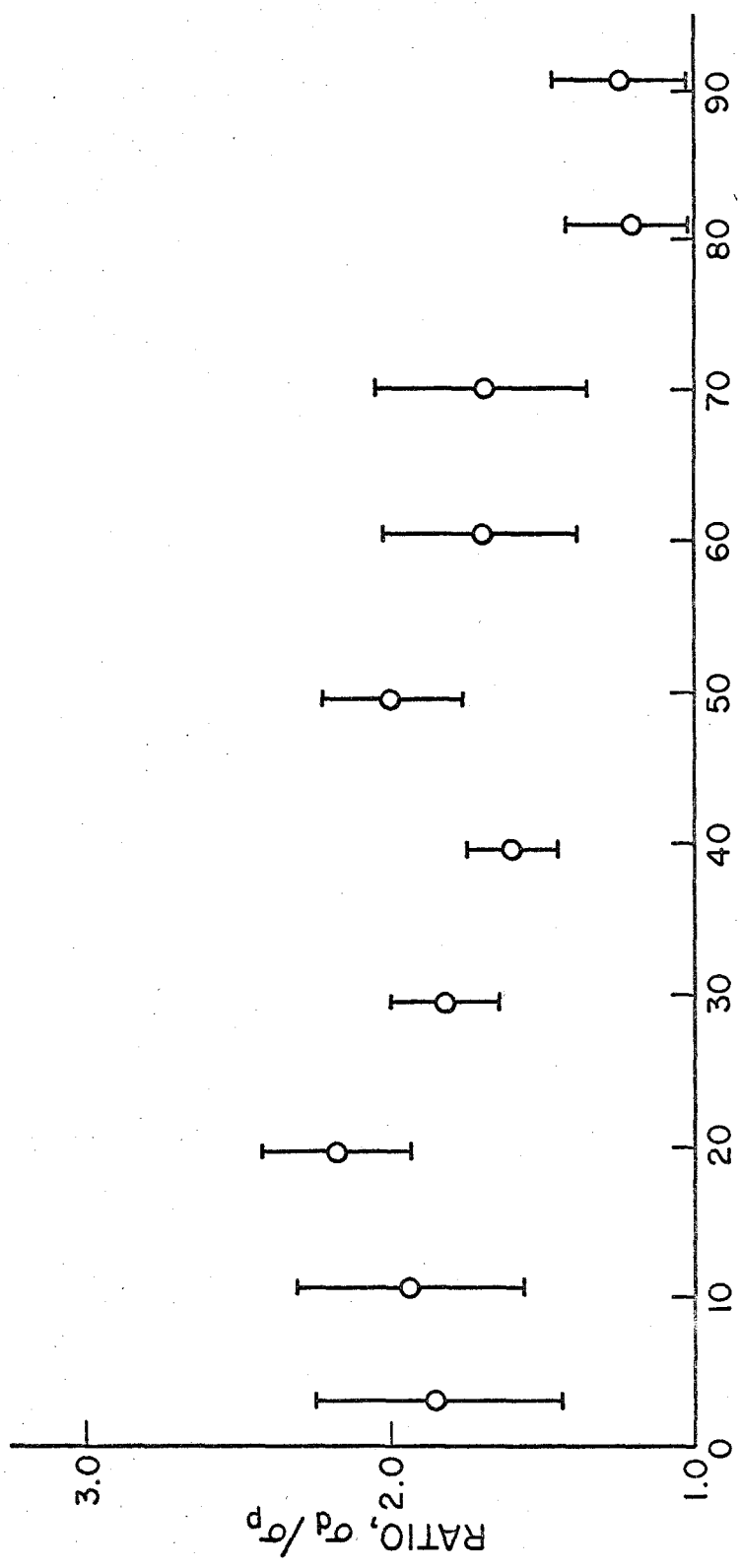

FIGURE 12c DEUTERON-PROTON CROSS SECTION RATIO, $\bar{K}$ = 1390 MEV

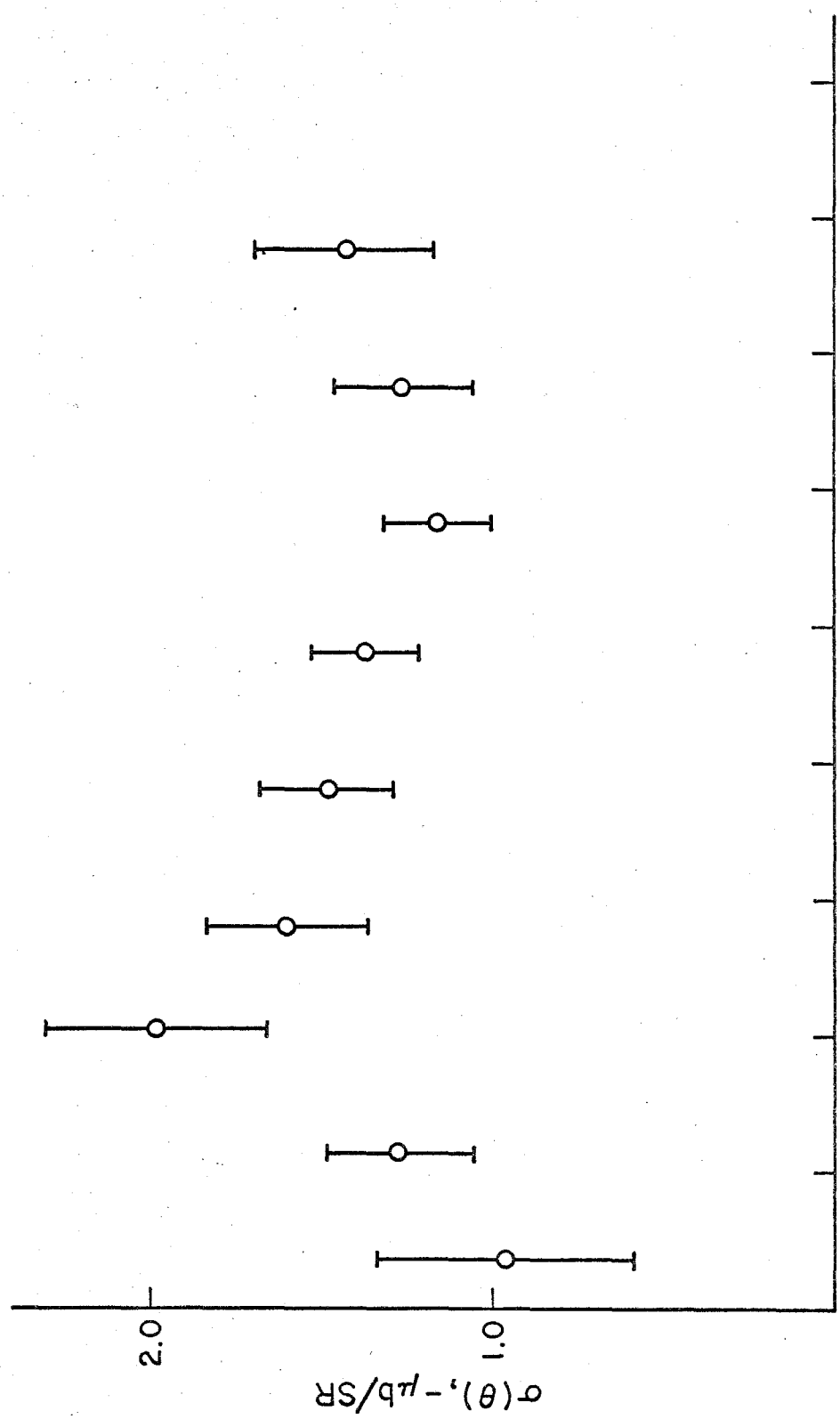

FIGURE 13a π^0 PHOTOPRODUCTION CROSS SECTION $\gamma + n \rightarrow \pi^0 + n$, $\bar{K} = 911$ MEV

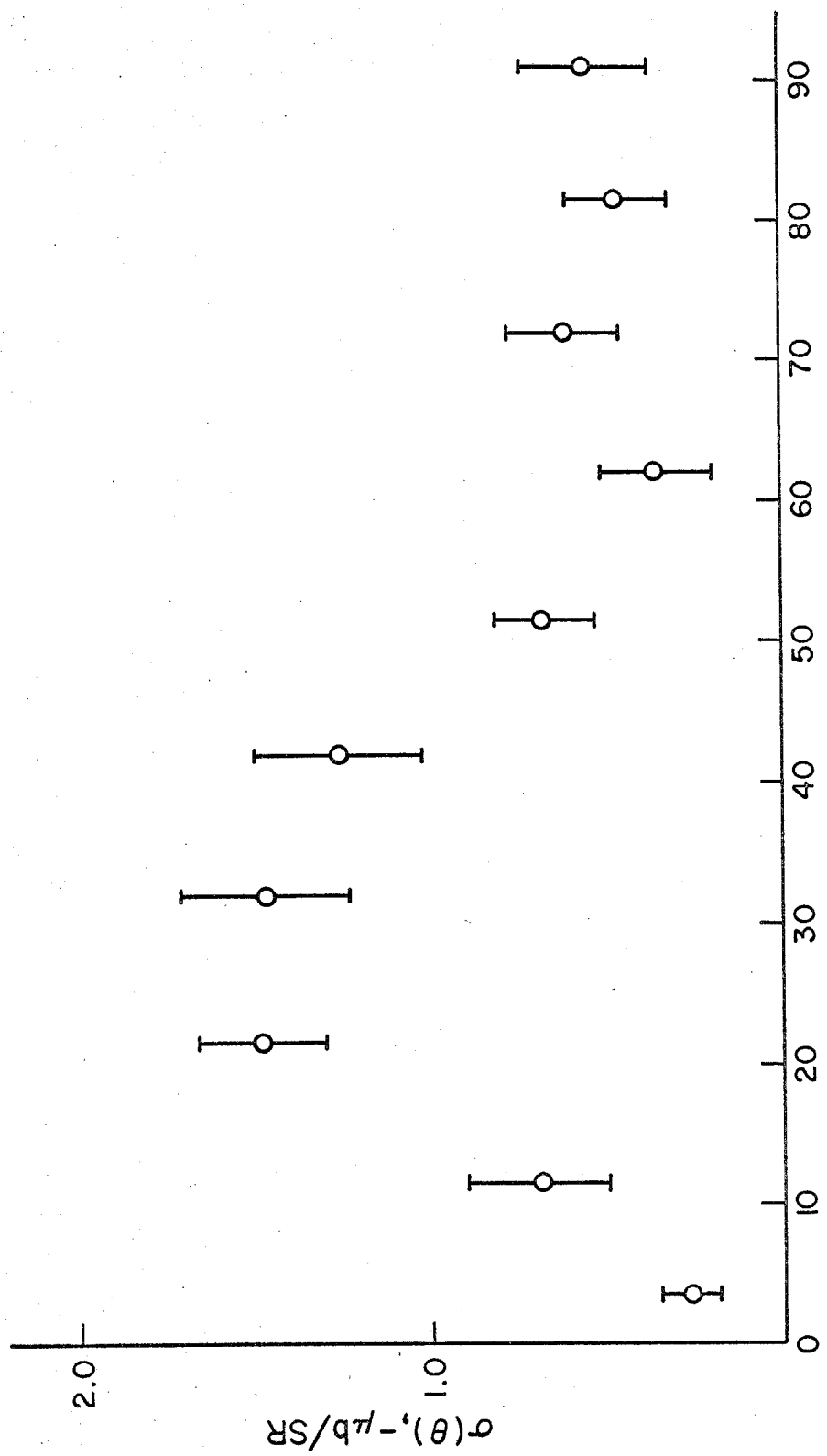

FIGURE 13b π^0 PHOTOPRODUCTION CROSS SECTION $\gamma + n \rightarrow \pi^0 + n$, $\bar{K} = 1182$ MEV

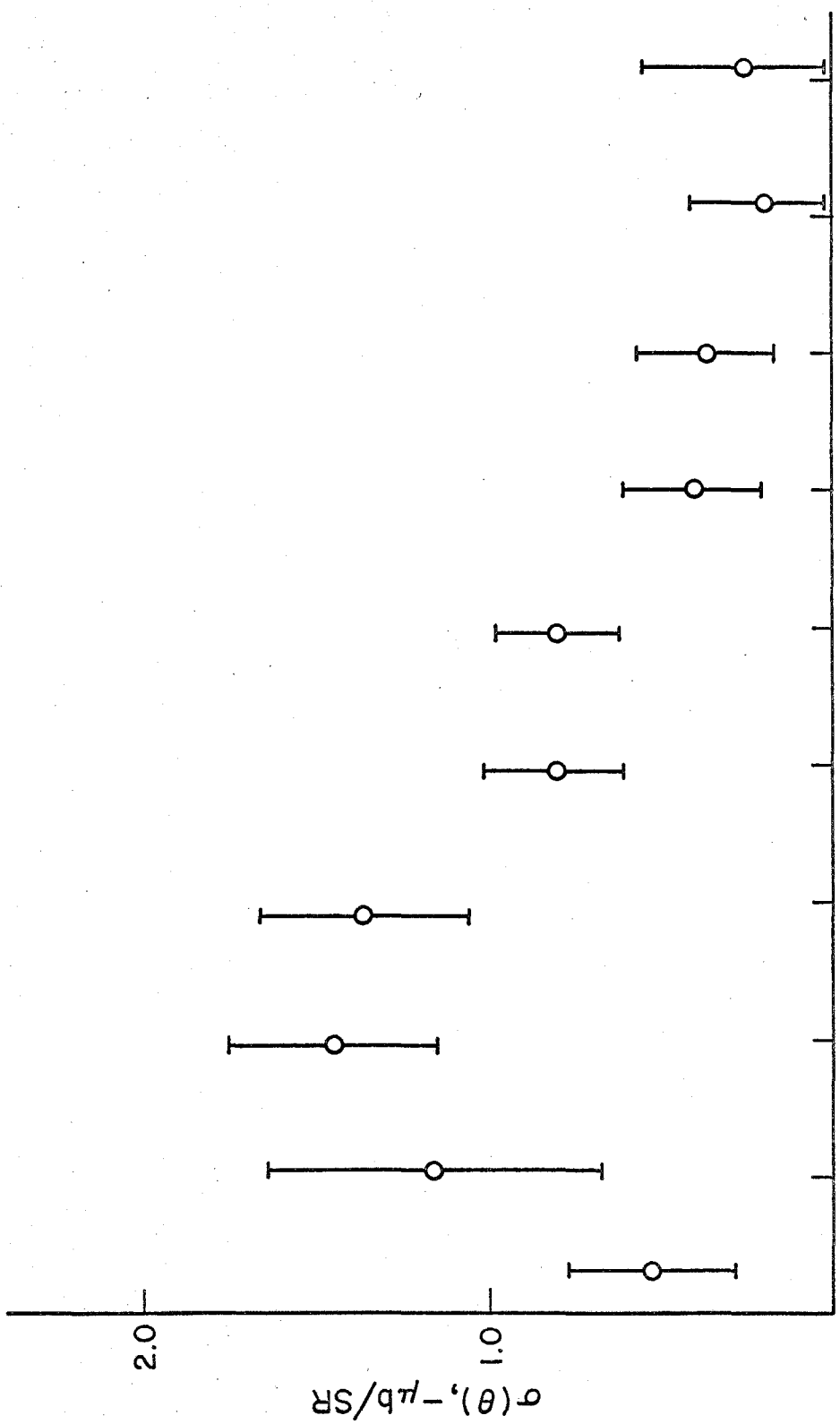

FIGURE 13c π^0 PHOTOPRODUCTION CROSS SECTION $\gamma + n \rightarrow \pi^0 + n$, $\bar{K} = 139$MEV

VI. DISCUSSION OF RESULTS

The analysis of results from deuteron targets utilizes the impulse approximation[8, 9] which takes the T matrix elements for a bound nucleon target to be equal to those for a free nucleon. The condition for validity of this approximation is that the energy of the incident particle be large compared to the binding energy of the nucleons in the target particle. The deuteron binding energy is 2.2 MeV, while the incident photon or outgoing pion energy is about 1000 MeV. Clearly the impulse approximation can be used. The analysis must then take into account:

1) the interaction of the two nucleons in the initial and final states,

2) the interaction of the produced pion with the second nucleon, or multiple scattering.

If 2) is neglected, the T - matrix may be written[8]

$$T_D = \langle f | T_p + T_n | i \rangle \ .$$

We define

$$T = \mathcal{A} + \sigma \cdot \underline{K}$$

D = average recoil of the two nucleons

$$F(D) = \int u_d^2(r) \exp(i\underline{D} \cdot \underline{r})$$

$U_d(r)$ = radial wave function of the deuteron.

The cross section obtained from this definition for the T matrix is

$$\frac{d\sigma}{d\Omega} \approx \frac{1}{2\pi}\left[\mathscr{L}_p^2 + |\underline{K}_p|^2 + \mathscr{L}_n^2 + |\underline{K}_n|^2 + 2F(D)\mathrm{Re}\left(\frac{1}{3}\underline{K}_n^* \cdot \underline{K}_p + \mathscr{L}_n^* \mathscr{L}_p\right)\right]$$

which is the sum of the free nucleon cross sections plus an interference term whose size depends upon the deuteron overlap integral F(D). F(D) is given in Figure 14 as a function of recoil D, and of CM pion angle for $\bar{K}$ = 1182 MeV. Since cross section data alone are insufficient to determine the four independent production amplitudes $(\mathscr{L}, \underline{K})$, the equation cannot be used to determine a neutron cross section. However, the size of the interference term may be estimated since $\mathscr{L}^2$, $|K|^2 < d\sigma/d\Omega$. The rapid fall off of F(D) implies that the deuteron cross section is equal to the sum of the free proton and neutron cross sections to better than 5 per cent for CM angles greater than 20 degrees, so the simple "spectator model" is a valid approximation here.

The treatment of multiple scattering obtains the equation[9, 10]

$$\frac{d\sigma}{d\Omega} = \frac{d\sigma^p}{d\Omega} + \frac{d\sigma^{p'}}{d\Omega}\,\frac{1}{R^2}\,\frac{d\sigma^s}{d\Omega}$$

where R is the radius of the scattering system defined by $R = \int RU^2(R)dR$ and $d\sigma^p/d\Omega$ and $d\sigma^s/d\Omega$ are the production and scattering cross sections respectively. The principal contribution from the scattering term $\frac{d\sigma^p}{d\Omega}\,\frac{1}{R^2}\,\frac{d\sigma^s}{d\Omega}$ will arise from charged meson

production followed by exchange scattering, since the ratio of charged to neutral pion production cross sections is large. The size of the correction at 0^{o} can be estimated as follows. The charged pions which can scatter with sufficient energy to be detected by the experimental resolution function define a production solid angle $\Delta\Omega_p$. The solid angle for scattering is $\Delta\Omega_D$, the solid angle of the detector. (Note $d\sigma^S/d\Omega$ is in the laboratory frame.) Then the ratio of direct pions to scattered pions is

$$\alpha = \frac{\frac{d\sigma^{\pm}}{d\Omega}^{*} \times \Delta\Omega_p \times \frac{1}{R^2} \frac{d\sigma^S}{d\Omega_L} \times \Delta\Omega_p}{\frac{d\sigma^o}{d\Omega}^{*} \times \Delta\Omega_D} = \frac{\frac{d\sigma^{\pm}}{d\Omega}^{*}}{\frac{d\sigma^o}{d\Omega}^{*}} \times \frac{\Delta\Omega_p}{R^2} \times \frac{d\sigma^S}{d\Omega}_L .$$

The kinematics limits $\theta_{\pi^{\pm}} < 20^{o}$, so $\Delta\Omega_p \approx 0.5$ steradians. Thus $\alpha = 25 \times 0.5 \times 1/100 \times 5 = 0.5$. Multiple scattering effects can, then, give the observed $\gamma + d \rightarrow \pi^{o} + d'/\gamma + p \rightarrow \pi^{o} + p$ ratio at small angles with $\sigma_p \approx \sigma_n$. To obtain a neutron cross section from the deuteron photoproduction data will require 1) all the scattering cross sections such as $\pi^{+} + n \rightarrow \pi^{o} + p$, which can be obtained from phase shift analyses giving both isospin 1/2 and isospin 3/2 states, 2) computer calculation of the contribution at each data point, and 3) estimation of the higher order terms in the series.

Previous experiments which have measured the ratio $R_o = \pi^{o}(d)/\pi^{o}(p)$ are those of Chang[16] and Bingham[17], both in the energy region less than 1000 MeV. The results of Bingham show

the ratio at 60 degrees near 900 MeV to be about 1.95 +- 0.05, in disagreement with our result. The results of Chang show ratios more in accord with ours, but his results are at energy intervals which are too wide to permit detailed comparison. For example, at 870 MeV he finds R = 1.71 +- .14 at 60 degrees, and R = 1.62 +- 0.2 at 90 degrees.

The general character of the results obtained by this experiment shows a ratio which decreases with increasing angle. At small angles, the ratio decreases with increasing photon energy. In view of the final state interactions discussed above, we believe that even semi-quantitative conclusions about the neutron cross section will require more theoretical work on the effects introduced by the use of a deuteron target.

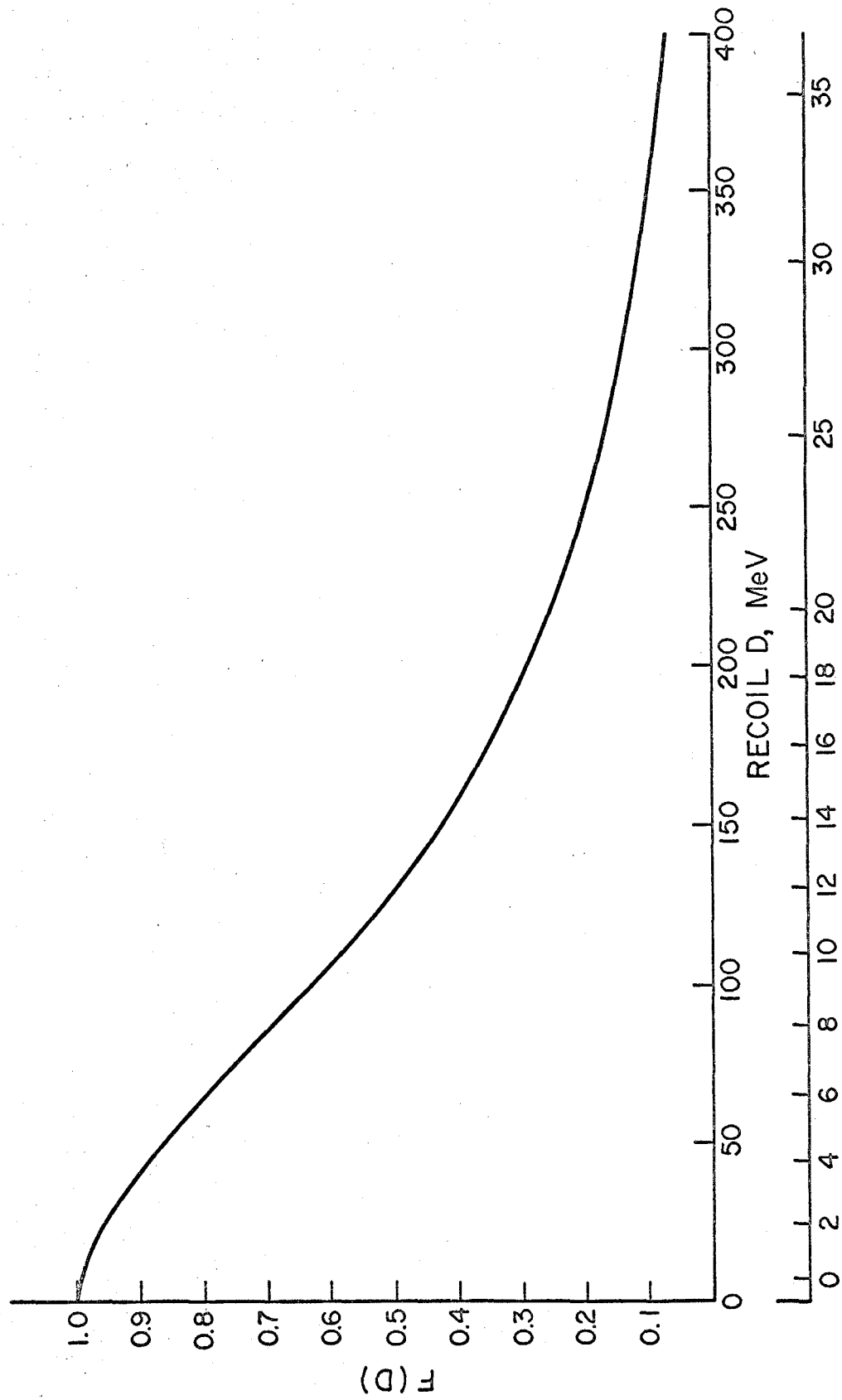

Figure 14 DEUTERON OVERLAP INTEGRAL

APPENDIX I. EXPERIMENTAL APPARATUS

A. Cherenkov Counters

Each Cherenkov counter[4] is constructed from two lead glass parallelepipeds 14 x 12 x 6 inches joined by α-bromo-naphthelene matching liquid to make a single optical block. The mounting house is made of soft iron, serving to shield the counter both optically and magnetically as well as support the lead glass and the 9 RCA 7046 phototubes which viewed it. The construction is shown in Figure 15. The Cherenkov counter is sufficiently large that, with the aperture used, the entire shower is contained in the glass. Statistical fluctuations on the shower production are therefore a small effect. The width of the pulse-height distribution is assumed to be due to the statistical production of photoelectrons by a constant number of Cherenkov photons. For n photoelectrons the pulse height is given by $\mu = \alpha n$, and the width by $\sigma = \alpha\sqrt{n}$. The relation $(\mu/\sigma)^2 = n$ allows the determination of the number of photoelectrons produced by each tube. The results of the tests in the mono-energetic electron beam are shown in Figures 16 and 17. They show:

1) linear average response in energy,

2) a response function which is nearly Gaussian with a width corresponding to 220 photoelectrons/GeV.

For each tube we have for the distribution of photoelectrons

$$D(n) = \frac{1}{\sqrt{2\pi n_o}}\, e^{-(n - n_o)^2/2n_o} \quad \text{or} \quad D(\mu) = \frac{1}{\sqrt{2\pi\alpha\mu_o}}\, e^{-(\mu - \mu_o)^2/2\alpha\mu_o}.$$

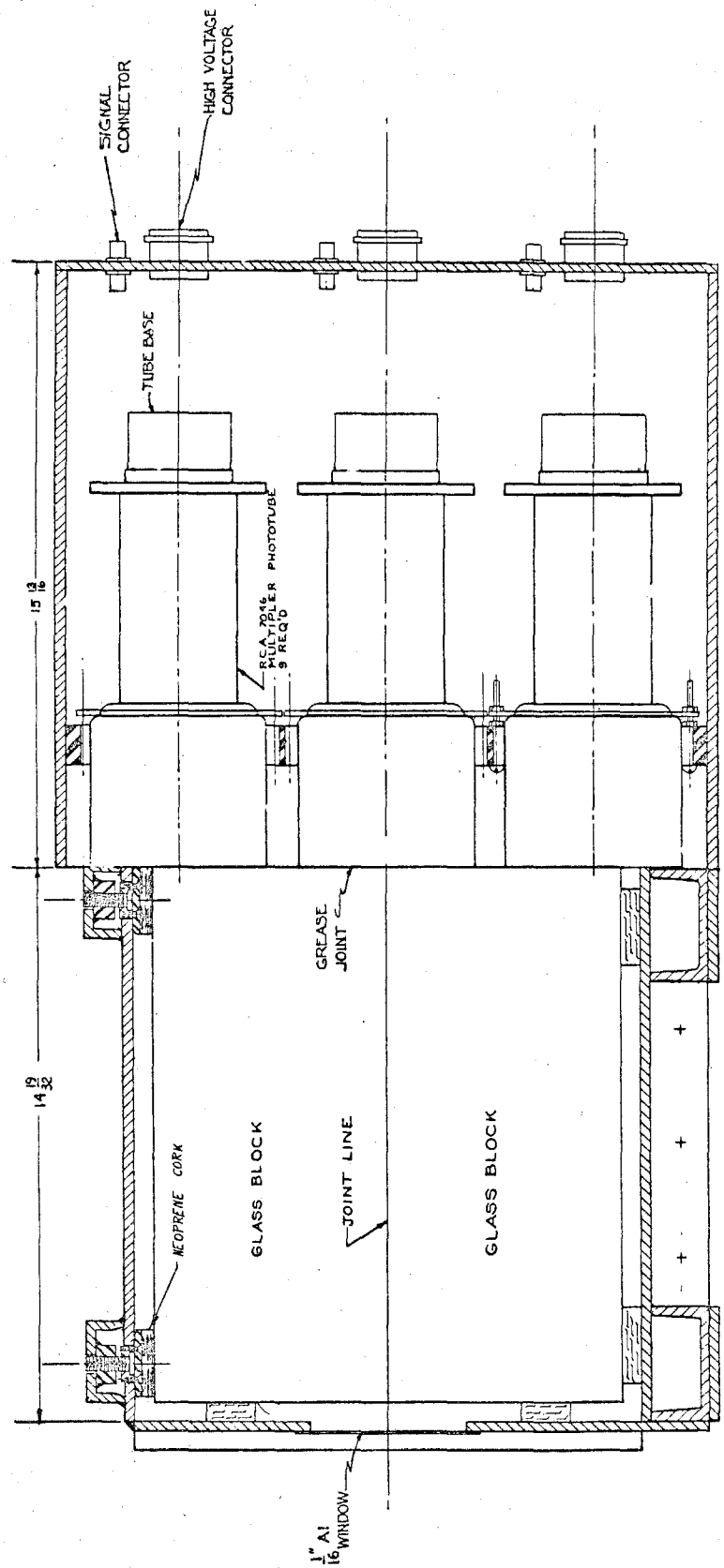

FIGURE 15 V CERENKOV COUNTER ASSEMBLY SHOWING DETAILS OF CONSTRUCTION AND PHOTOTUBE MOUNTING.

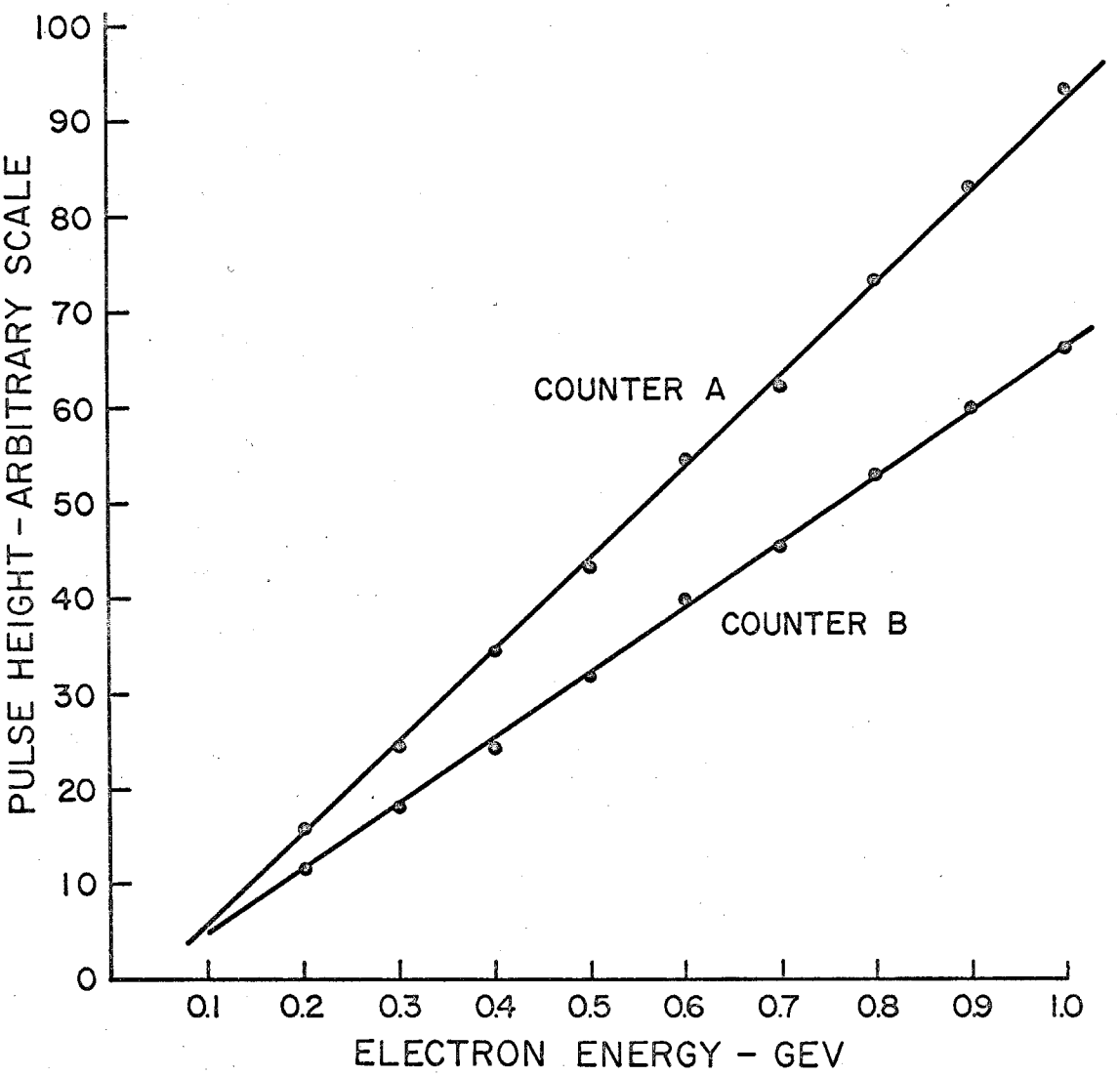

FIGURE 16 $\overset{v}{C}$ COUNTER RESPONSE

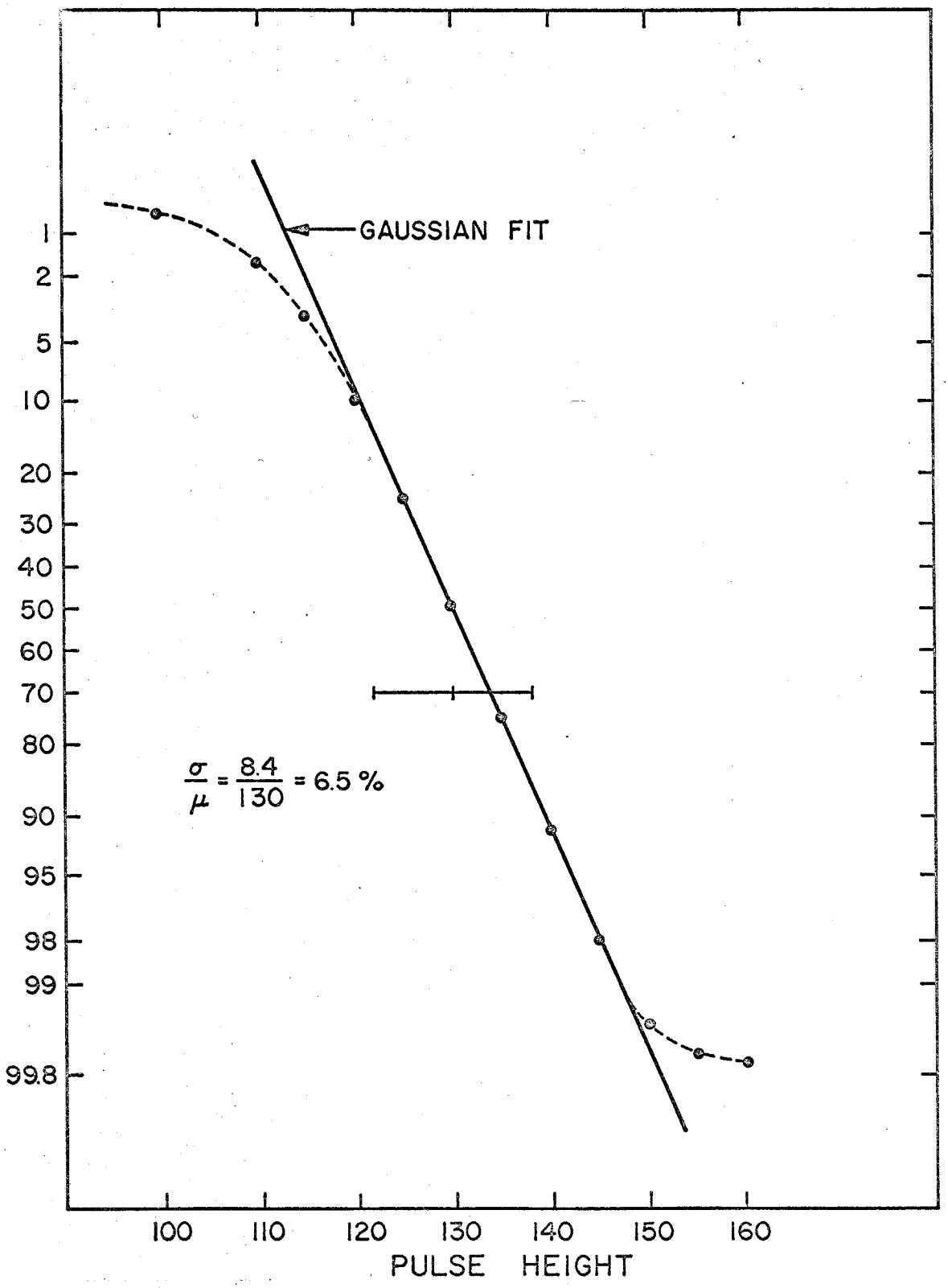

FIGURE 17 $\check{C}^{V}$ COUNTER RESOLUTION FUNCTION

If the assumption of width source is true, minimum width of the distribution obtained by summing the outputs of the nine tubes is achieved by setting the average pulse height of each tube proportional to the number of photoelectrons it produces. Thus we have $\mu_i = \alpha n$, $\mu_i = \alpha \Sigma n_i$, $(\frac{\mu}{\sigma})^2 = \Sigma(\frac{\mu_i}{\sigma_i})^2$ or $N = \Sigma n_i$. In actual test in the mono-energetic electron beam the array gave 220 photoelectrons, compared with 250 photoelectrons from summing the result of each tube. The decrease is most probably due to incorrect setting of the gain of the tubes, rather than statistics on the shower. The response and linearity of the counters have not been measured for mono-energetic photons. The mechanism of shower production by electrons is the same as that for photons so we have taken the results to be identical. The agreement of observed and computed spectra for photon energies near 650 and 1350 MeV (80°, 911 MeV and 10°, 1390 MeV) indicates that the conclusion is valid.

A convenient scale on which to record pulse height will be in energy. Since the mean pulse height produced by the counter is a linear function of energy, $\mu_o = kE_o$, only a scale change is necessary. The distribution of pulse height can be written

$R(E, E') = \frac{1}{\sqrt{2\pi kE}} e^{-\frac{(E' - E)^2}{2kE}}$, where E is the photon energy, and E' is the output on the energy scale. We use this scale throughout the thesis.

During the tests in the electron beam, the output of the counters on cosmic ray muons traversing the glass block was also measured. The energy equivalent of the produced Cherenkov light

was found to be 220 MeV for each counter. Since this number is a function only of the lead glass, its daily measurement provides a useful check on the gain of the phototubes, i.e., on the constant which will be used to connect the energy and pulse-height scales.

In use, the counters were mounted one above the other on a trolley movable at constant radius about the target to any angle measured. The system, designed by Mr. Edward Taylor, was so delicately balanced that it could be moved at the rate of 10^{o} per minute by a single graduate student using a four foot wrecking bar. Each counter could be moved independently in the vertical direction to obtain any desired displacement about the beam plane. Tape measure and fiducial marks allowed setting angles to better than 0.1^{o} and distances to 1/32 inch or better. The counters were surrounded on five sides by lead walls. The front walls were eight inches thick, the remaining walls four inches thick. With the apertures blocked, counting rates in the veto scintillators and the Cherenkov counter were negligible. The aperture size varied from 5" x 7" to 8" x 8". The variation in average pulse height as a function of position on the counter face was measured in the electron beam[3] and found to be less than ± 4 per cent over the maximum aperture used.

B. The Aperture Veto Telescope

Each aperture was backed by a two counter telescope to veto charged particles. The counters were separated by two grams of CH_2 absorber. The rate in a single scintillation counter is principally due to Compton electrons produced in the scintillator by the halo of low energy photons produced by the collimation of the bremsstrahlung beam.

These electrons, up to 15 MeV in energy, will be stopped by the absorber and hence do not contribute to the veto rate. The low energy photon halo is negligible at angles greater than 20^{o} (lab). The efficiency of the veto system was measured by means of a small counter in coincidence with the Cherenkov counter and found to be better than 97 per cent at the highest rates encountered. The phototubes used were RCA - 7850. The capacitor bank supplying dynode power was boosted by external power supplies on the last two dynodes. At two megacycle counting rate, the drop in pulse height at the end of the 150 millisecond dump was measured to be less than 5 per cent.

C. The Condensing Target

The construction of the condensing target is shown in Figure 18. The target consisted of the vacuum chamber, the jacket, and the appendix itself. The housing windows and appendix end caps were of clear mylar, 5 and 1.5 mil thickness respectively. The clear mylar allowed visual inspection of the state of the appendix. In use, the jacket was filled with liquid hydrogen at atmospheric pressure. Supply was a commercial hydrogen dewar, pressure fed to the jacket. The pressure feed valve was either on or off, and was controlled by the jacket temperature sense resistor. The sensitivity was variable. While operating, the valve was set such that the system did not oscillate, simply filling the jacket to replace hydrogen lost by boil off. Gaseous hydrogen or deuterium was put into the jacket under four pounds pressure. The rate of condensation with these parameters required about one hour to fill the appendix, and consumed about one liter of liquid hydrogen. The appendix was

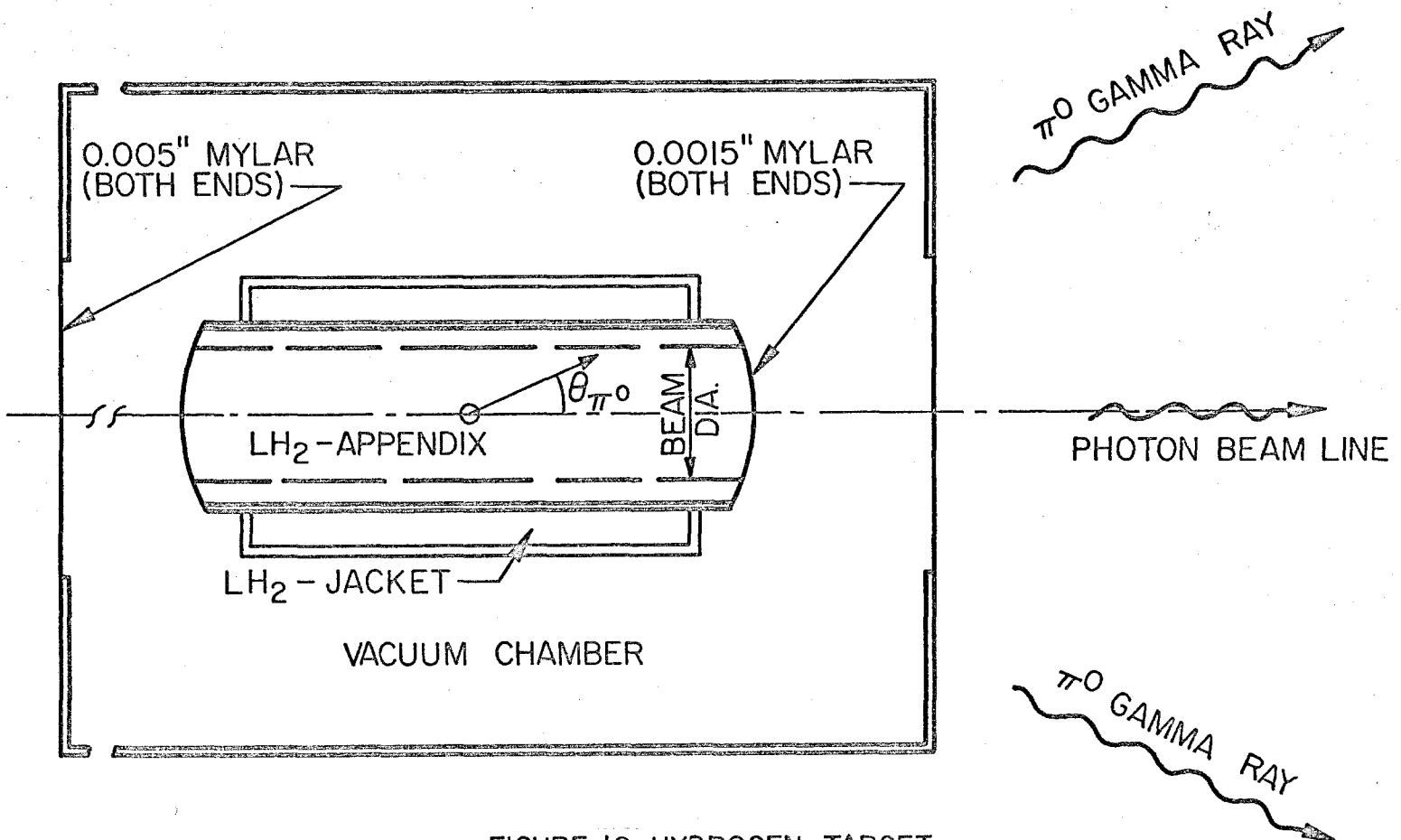

FIGURE 18 HYDROGEN TARGET

quiescent after filling. The appendix sense resistor was used only to check that the target was full. Steady state hydrogen consumption was about 0.9 liters per hour. Hydrogen for the appendix was obtained directly from commercial cylinders and discarded after each day's run. The cost required the deuterium to be contained between runs. The method used was an inflatable bag of about 500 liters capacity under four pounds positive pressure. This system was adequate for the fill and boil off rate of the target. Purity of deuterium from all gases but hydrogen was maintained by discarding the last few liters of deuterium during boil off. The density of hydrogen and deuterium was calculated assuming the appendix temperature to be that of boiling hydrogen at Pasadena STP (750 mm, 23° C.), or 20.1°K. At this temperature, the densities[11] are $\rho_{H_2} = 70.3$ gm/liter, $\rho_{D_2} = 169.7$ gm/liter.

D. Calibration of the System

The co-ordinates of the pulse-height matrix have been defined by the amplified and stretched Cherenkov pulse. From this matrix we wish a matrix with an energy scale which is the same for all runs which are to be combined. Let

E = Output of phototubes on the energy scale

V = Pulse height analysed

α = Gain of phototubes in Volts/MeV

G = Electronic gain of the system

The obvious equation relating these quantities is $E = (V/\alpha)/G$. The problem of obtaining the matrix in energy is non-trivial because 1) the electronic gain G is neither a linear function of E nor constant in time and may be different for the various configurations, and 2) the gain of the phototubes α is not constant in time. The calibration input at the phototube summer allows us to use a simulated Cherenkov pulse of known height to measure the electronic gain. The pulse was generated by an SKL pulser with an R-C network and duplicated the shape of the Cherenkov pulse sufficiently well to determine the gain over the range of energies measured. In particular, the extrapolation from the 220 MeV pulse height of cosmic ray muons to the maximum π^0 gamma-ray energy was assumed valid. The electronic calibration was measured daily, with short term drifts of 2 per cent observed. The stability of the SKL pulser and the ND analyser was checked by using a passive stretching network to produce 20 μsec pulses which could be put directly into the analyser. The pulser analyser combination was found to be stable to better than 0.2 per cent.

The average pulse height produced by cosmic ray muons was measured each day during the 12 hour period while the experiment was not run. Using the analyser in the 32 x 32 mode again allowed measurement of both counters at once. The muon pulse-height spectrum is nearly Gaussian in shape with a width of 12 per cent, so the mean value determined by the 1200 counts collected in 12 hours is of sufficient accuracy. Given the gain as measured by the previous paragraph, and the energy equivalent for muons obtained by comparison with the electron beam, both factors G and α have been determined and the matrix can be converted to one in energy.

APPENDIX II. DATA REDUCTION

We consider here the process of converting the counting data into a cross section, with errors introduced. The procedure is:

A) reduction of the output matrix in pulse height to a matrix in energy with a linear scale,

B) analysis of the consistency of the foreground, background, and accidental runs with discussion of electronic problems,

C) evaluation of the π^0 spectrum from the foreground, background, and accidental spectra as taken, to obtain the counting rate,

D) computation of the detection efficiency, including small corrections to the π^0 rate,

E) computation of the quoted cross section from the counting rate and the resolution function,

F) summary of the statistical errors,

G) estimation of the size of the systematic errors,

H) attempts to improve the energy resolution of the experiment.

A. Reduction of the Output Matrix

The raw data produced a 32 x 32 matrix in pulse height from the two Cherenkov counters. To be useful, this matrix requires considerable analysis which we describe in detail. The determination

of the matrix edges in energy is described in Appendix I, together with the uncertainty in the values. Given the edges in energy, the second step is generating a linear matrix with a given bin width from the nonlinear, nonequal matrix. To find the contribution to the new bin $\underline{s}$ from the given bin 2, 2, a six parameter surface is determined by the number of counts in the nine bins shown. Then, an integral of this function between (a_1, a_2) and (b_1, b_2) gives the contribution. Proceeding likewise for bins (2, 1), (3, 1) and (3, 2), the number of counts in bin $\underline{s}$ is found.

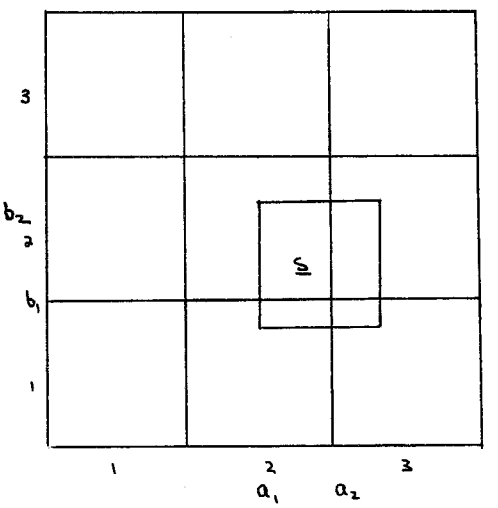

The initial choice of constant connecting energy with pulse height is given by the day's cosmic ray calibration. However, the data itself, assuming a reasonably slowly varying cross section, can be used to find this number by comparing the observed spectra with the computed spectra of Appendix IV. We have used the following procedure to do this.

1) Using the calibration given by the day's cosmic ray run, the linear matrix is generated with the desired energy scale for each foreground (F), background (B) and accidental (A) run. The result for π^0 from deuterium (π) is then obtained.

2) The mean energy for each counter on (π) is obtained for each (F) individually. This energy is given to about $\pm$ 2%, which is better than the value given by the cosmic ray calibration. The photo-

tube gain is then changed to bring the mean energy in each counter to the value computed. From all (F) runs, we have the daily gain. The number is distributed about its mean with a width of about 2%. The (A) and (B) runs are then recomputed using the new gain figures. The procedure converges quickly to a consistent set of daily gain figures.

B. The Data

1. Foreground runs

The foreground rates are given in Table 11 in Appendix III together with χ^2 values for multiple runs. The overall χ^2 for the experiment is 122 for 134 degrees of freedom, but the values do not follow a χ^2 distribution very well. The cross comparison of runs done in the several configurations is given in Table 5.

2. Background data

We present the background cross-section ratio in Table 6. The data showed no statistically significant time variation in background rate for the 1073 and 1308 MeV data. Somewhat improved χ^2 values for individual (π) runs are obtained if foreground and background runs are combined from the same configuration. The runs were done in such sequence that this is always possible. The 1500 MeV data show a pronounced difference in background for the small angle, wide radius configuration when compared with overlapping points at the same angle for the narrow radius. These points were taken during a period of poor beam collimation due to instabilities in the synchrotron circulating beam at an endpoint of 1513 MeV.

TABLE 5

Comparison of Experimental Configurations

Position	Counting Rates Pions/BIP 1	2	Efficiency Ratio	Cross Section Ratio
D_2, 1073, 20°	1.86(0.08)	2.66(0.14)	1.33	1.07(0.08)
1073, 28°	1.41(0.05)	2.24(0.06)	1.52	1.04(0.05)
1512, 17°	0.54(0.04)	1.32(0.10)	2.38	1.02(0.12)
H_2, 1073, 28°	0.65(0.03)	0.99(0.04)	1.52	0.99(0.06)
1308, 11°	0.21(0.15)	0.34(0.03)	1.65	0.98(0.12)
1512, 11°	0.23(0.02)	0.48(0.03)	2.31	0.92(0.08)
1512, 17°	0.62(0.05)	0.26(0.03)	2.35	1.02(0.10)
			Average	1.01(.03)

TABLE 6

Background/Foreground Ratio

E_o = 1070 MeV		1308 MeV		1510 MeV	
Angle	Ratio	Angle	Ratio	Angle	Ratio
0.0	0.08	0.0	0.20	0.0	0.15
5.0	0.1	5.0	0.20	5.0	0.125
10.0	0.12	10.0	0.085	9.5	0.145
15.0	0.06	17.0	0.042	15.0	0.150
20.0	0.04	22.0	0.05	20.0	0.074
28.0	0.04	28.0	0.05	26.0	0.032
35.0	0.053	35.0	0.05	32.0	0.09
42.0	0.053	42.0	0.06	39.0	0.10
49.0	0.067	49.0	0.065	46.0	0.10
		56.0	0.064	53.0	0.11

Comparison of the (π) rates, subtracting backgrounds from the same configuration, gives reasonable χ^2 values so no error has been added to the final rate.

The ratio of background to foreground cross sections at wide angles show that the counters viewed about 0.2 grams of material. The four mylar windows of the target contribute 0.04 grams. The remaining 0.16 grams corresponds to 130 cm of air. The counter geometry shows this to be a reasonable figure. The rise in the forward direction is due to two effects. The secondary scrapers become visible from the apertures, and coherent production from the complex nuclei in the background material becomes large.

3. Accidental coincidences between the Cherenkov counters

The rate of accidental π^o coincidences (γ_A + 100 ns) · (γ_B) was monitored constantly. At points needing correction, the accidental π^o spectrum run was taken by delaying γ_A through the π^o coincidence circuit. The rates γ_A and γ_B were checked for consistency between the (F) and (A) runs. The gamma rate is governed principally by two variables. 1) The energy bias set on the Cherenkov counters by the discriminator gives a low energy cutoff to the analysed pulse height. 2) The beam alignment through the secondary scrapers affects the shape of the scattered photon spectrum, especially for low energies. It is not possible to express the accidental rate as a function of γ_A and γ_B in a simple way. However, Table 7 shows that the simple product of the rates gives a correct measure to a factor of two which is sufficient to provide a check, and to prove that points for which a spectrum was not taken do not, in fact, need a correction.

TABLE 7

Accidental Rates

R = accidental rate

$\gamma_{A,B}$ = rate in each Cherenkov Counter

I = relative beam intensity

α = proportionality constant

$R = \gamma_A \times \gamma_B \times I^2 \times \alpha$

	Angle	I	Rate	$\gamma_A \times \gamma_B \times I^2$	α
H_2	0	1.0	0.02	25	0.8
	5	1.0	0.07	70	1.0
	10	2	0.08	120	0.7
	15	1.7	0.013	19	0.7
	20	1.7	0.01	10	1.0
	28	2	0.01	20	0.5
D_2	10	2.5	0.12	150	0.8
	15	2.5	0.13	180	0.7
	20	2.5	0.09	120	0.8
	28	1.0	0.014	20	0.7

4. Electronic problems

We have considered accidental π^0's in the third section. The problem of accidentally vetoed gamma rays is a straightforward correction, knowing the veto rate and the width of the veto discriminator pulse. At the maximum veto rate of 200 kc and the 20 ns pulse width, both sides will veto 1.2 per cent of the gamma rays. The veto rate was monitored directly by means of coincidences between γ and V. This monitor gave a correction of less than 2 per cent.

The dead time in the veto discriminator was 30 ns per pulse. At the 200 kc veto rate, 1.2 per cent of the vetos are missed. With the veto removed on one side, the π^0 counting rate increase was less than 10 per cent at all points. The source of the increase is consistent with the detection of a single π^0, one gamma ray of which converts in the aperture wall. Hence missed vetos can be ignored at all points.

C. Evaluation of the π^0 Spectrum

The three spectra which make up the data, foreground (F), background (B), and accidental (A) are shown in Figure 8, together with the resulting π^0 spectrum (π). The counting data have been tabulated in Table 11 for all the runs. The errors shown on the (F), (B), and (A) rates are their counting statistics. The number of counts is taken to be the number above the minimum in the spectrum, which usually occurs at an energy below which we calculate about 5 per cent of the counts lie. The numbers for (B) and (A) are taken at the same energy. This procedure gives a simple error analysis. The calibration for (B) and (A) was obtained as described in Section A) of this

Appendix. Since the rate depends on the energy scale, the errors introduced by the calibration procedure contribute to the counting rate error. The calibration error is statistically distributed with about 2 per cent width. The error introduced is given by the product (counts per MeV at cutoff) x (calibration error in MeV). These are combined and given in Table 11 in Appendix III.

The final (π) spectrum does not show a complete separation between the π and $\pi\pi$ regions. The correct procedure here is to fit to the complete spectrum a function in two parts, the single π^0 spectrum shape from Appendix IV, including single π^0 detection in double π production, and the semi-phenomenological shape for $\pi^0\pi^0$ from Appendix V. However, the approximation of taking the number of counts above the minimum channel is good to better than 3 per cent except for the point (0^0, 1073), the loss in π^0 being equal to the gain in $\pi^0\pi^0$. The error in the exact procedure is due to counting statistics on ($\pi\pi$) below the cutoff. This number is quite well given by the number of counts per 25 MeV at the cutoff channel. The systematic error introduced by the choice of fitting function for ($\pi\pi$) is less than 1 per cent, by comparing several choices for the function.

D. Calculation of the System Detection Efficiency

1. The geometric efficiency

We define η_A = the result of the analytic efficiency calculation

η_M = the result of the Monte Carlo calculation

η = the true efficiency.

The detection efficiency at the various angles of the same configuration is given to about 10 per cent by

$$\eta(\theta_{\pi}) = \alpha \times \left(\frac{d\Omega_{cm}}{d\Omega_{lab}} (\theta) \right) \times \frac{dp}{d\varphi}$$

where $d\Omega_{cm}/d\Omega_{lab}$ is the production solid angle transformation and $dp/d\varphi$ is the decay probability for a π^o, taking the decay angle φ to be the mean angle of the aperture with the beam plane. This is the expression of the fact that the counters appear the same in the center of mass at all angles. (Note that this comparison is made with values of η_A for the same photon cutoff energy, not the real values which vary slightly from one to the other.) The relation makes it reasonable to write $\eta(\theta) = \beta \times \eta_A(\theta)$ and find β by a minimum χ^2 method using the results of the Monte Carlo program which are distributed about the true value with known error. The errors on the Monte Carlo calculation are typically on 2500 successes, or 2 per cent, so the value for η is certainly known to better than 1 per cent.

2. Corrections to the π^o rate

a) Effective aperture size

The lead walls transmit some of the gamma rays, so the effective aperture size is greater than the geometrical aperture size. We have

$$\eta = \eta_o + \left.\frac{d\eta}{dx_1}\right|_o x_1 + \left.\frac{d\eta}{dx_2}\right|_o x_2 + \left.\frac{d\eta}{dx_3}\right|_o x_3$$

where x_1, x_2, x_3 are the displacements at the outside, inside, and sides of the apertures. If the gamma ray makes an angle θ with the lead wall, the traversed distance is $\delta = x/\sin\theta$ and the absorption is $\varphi(\delta) = e^{-\tau\delta}$ where $\tau = 1.4\ \text{cm}^{-1}$. To first order, then,

$$\Delta\eta = \int \frac{d\eta}{dx}\, e^{-x\tau/\sin\theta}\, dx$$

$$= \left.\frac{d\eta}{dx}\right|_o \times \frac{\sin\theta}{\tau}$$

or the effective aperture size is defined by $x_e = x_o + \sin\theta/\tau$ for each x. The apertures are shaped on sides x_2 and x_3 so $\sin\theta/\tau < 0.1$ cm. Side x_1 is not shaped and has a large derivative since the separation determines the cutoff energy. The efficiencies were calculated at each point with the corrected aperture size to give the correction.

b) Conversion of π^o gamma rays

The materials which the gamma rays traverse are: the walls of the target and vacuum chamber, the air path, and the front scintillation counter. Referring to Figure 18, the target is of a complex shape requiring a ray trace at each angle to find the path length.[3] For example, at 28 degrees laboratory angle, traversing all of the aluminum layers gives a total path length of 0.62 cm, or an absorption of 5 per cent per gamma ray. The maximum absorption correction is 6.8 per cent per gamma ray. The results of the ray trace are integrated over the finite target to obtain the correction.

Taking $\tau = 2.3 \times 10^{-5}$ cm^{-1} the absorption by the air path is 0.23 per cent per 100 cm., or 0.7 per cent per gamma ray. To be counted in the front scintillation counter the bias set on the counter pulse height required a path length of 0.3 cm for the produced electron pair. The length for conversion is then 0.85 cm, so taking $\tau = 0.185$ cm^{-1} we have 1.6 per cent per gamma ray.

c) Shadowing correction

At the non-standard radii the apertures did not rotate about the target center, so at some angles not all of the apertures could be seen from the target. The correction is just geometric.

Table 8 gives all the efficiencies with average angles, photon energy, and cutoff energy. Also given is the factor from the corrections just discussed which multiplies the geometric efficiency to obtain the system efficiency. Finally, the factors connecting BIP's with total beam energy[12] and the actual amount of target material must be used. These are given by

$$\eta(\text{system}) = \eta_o \times \left\{ \begin{matrix} 1.16 \text{ gm. hydrogen} \\ 2.795 \text{ gm. deuterium} \end{matrix} \right\}$$

$$\times \left\{ 1.10 \text{ Machine BIP's per } 10^{13} \text{ MeV} \right\} .$$

TABLE 8a

Parameters at Experimental Points

E_o = 1170 MeV
R = 110"

Angle, Lab	Angle CM	K	E_π	Efficiency	Correction
0.0	3.5	925	925	0.511	0.955
5.7	11.2	924	920	0.503	0.936
11.3	20.3	925	907	0.477	0.921
16.0	28.0	918	884	0.457	0.909
21.8	47.2	922	855	0.413	0.897
28.0	47.2	922	826	0.352	0.886
		R = 82"			
22.8	38.9	925	859	0.656	0.795
29.1	48.7	911	811	0.566	0.839
35.1	57.4	899	765	0.460	0.878
42.1	67.3	899		0.349	0.852
49.7	77.5	904		0.249	0.773

TABLE 8b

Parameters at Experimental Points

E_o = 1308 MeV

R = 110"

Angle, Lab	Angle CM	K	E_π	Efficiency	Correction
0.0	3.7	1169	1169	0.279	0.959
5.7	11.4	1167	1160	0.276	0.949
11.3	21.4	1171	1143	0.254	0.932
17.1	31.9	1175	1113	0.223	0.917
22.8	41.8	1176	1071	0.193	0.904
28.0	51.6	1180	1028	0.197	0.898
35.0	61.6	1190	967	0.137	0.894
42.0	72.0	1189	896	0.127	0.898
49.0	81.6	1186	826	0.101	0.900
56.0	91.0	1189	762	0.071	0.904

TABLE 8c

Parameters at Experimental Points

E_o = 1510 MeV

R = 140"

Angle, Lab	Angle CM	K	E_π	Efficiency	Correction
0.0	3.1	1382	1382	0.161	0.968
5.0	10.5	1385	1377	0.154	0.919
10.1	20.2	1380	1349	0.157	0.851
15.3	30.1	1381	1312	0.143	0.772
		R = 110"			
9.5	19.0	1387	1360	0.334	0.956
14.6	28.8	1386	1323	0.311	0.939
20.2	39.2	1384	1296	0.280	0.926
26.0	49.6	1388	1206	0.214	0.916
32.4	60.3	1385	1126	0.176	0.908
38.7	70.2	1385	1045	0.135	0.909
46.1	80.8	1388	954	0.091	0.915
53.0	90.7	1385	872	0.071	0.919

E. The Quoted Cross Section

We let C = the observed counting rate

$T(k,\theta)$ = the geometric resolution function

$\sigma(k,\theta)$ = the differential cross section

Then $C = \int \sigma(k,\theta)T(k,\theta)dk\, d\theta$.

The efficiency is defined by $\eta(\theta_o) = \int T(k,\theta)dk\, d\theta$

the mean photon energy by $k_o = \langle k \rangle = 1/\eta \int k\, T(k,\theta)dk\, d\theta$

and the mean pion angle by $\theta_o = \langle \theta \rangle = 1/\eta \int \theta\, T(k,\theta)dk\, d\theta$.

The cross section quoted is defined as $\sigma(k_o,\theta_o) = C/\eta$.

We now examine the effect of the energy-angle dependence of the cross section. Expanding the cross section to second order, and dropping the *- notation,

$$\sigma(k,\theta) = \sigma(k_o,\theta_o) + \sigma_k(k - k_o) + \sigma_\theta(\theta - \theta_o) + \sigma_{k\theta}\delta^2_{k\theta} + \sigma_{kk}\delta^2_{kk} + \sigma_{\theta\theta}\delta^2_{\theta\theta} .$$

Then the counting rate is

$$C = \eta \times \left\{ \sigma(k_o,\theta_o) + \frac{1}{2}\sigma_{kk}\langle (k - k_o)^2 \rangle + \frac{1}{2}\sigma_{\theta\theta}\langle (\theta - \theta_o)^2 \rangle + \sigma_{k\theta}\langle (k - k_o)(\theta - \theta_o) \rangle \right.$$

where the linear terms are zero by definition. The moments of the function T are given in Table 9, together with the values for the cross section derivatives in the following three cases: 1) the cross section due to the third pion-nucleon resonance alone, taking an $f_{5/2}$ Breit-Wigner resonance, 2) the data of Diebold[13] at 60 degrees, and 3) the data of this experiment at rather wide energy intervals. The corrections are

	Resonance	Diebold	This Expt
1) $\sigma_{\theta k}\delta^2_{\theta k}$	1.0%	-	0.3%
2) $\frac{1}{2}\sigma_{\theta\theta}\delta^2_{\theta\theta}$	1.3%		
3) $\frac{1}{2}\sigma_{kk}\delta^2_{kk}$	14%	15%	6%

Correction 1) may be ignored due to the small value of $\delta^2_{k\theta}$, which reflects the fact that k and θ are nearly independent variables for the two photon detection scheme. 2) is not quite ignorable, but the data comprise a distribution in θ so the value of $\sigma_{\theta\theta}$ may be estimated and a correction made. Correction 3) due to energy variation alone is not ignorable. If the cross section has the large but physically possible derivative indicated by the resonance, our data must be used with care. A systematic error has been added to the data for this effect.

TABLE 9

Cross Section and Resolution Function Parameters

Parameters for $\bar{k} = 1180$

$$\delta^2_{xy} = \langle (x - x_o)(y - y_o) \rangle$$

Moments

θ_{CM}	$\delta^2_{\theta k}$ MeV-Deg	$\sqrt{\delta^2_{\theta\theta}}$ Deg	$\sqrt{\delta^2_{kk}}$ MeV
0	47.0	2.10	72.7
30	52.4	1.57	71.0
60	67.1	1.58	67.8
90	90.1	1.60	69.6

Derivatives

Angle, CM	$\sigma_{k\theta}$	$\sigma_{\theta\theta}$	σ_{kk}
	Resonance		
0	0	3.8×10^{-3}	5×10^{-5}
30	2.5×10^{-4}	7.8×10^{-3}	5×10^{-5}
60	-2.3×10^{-4}	1.4×10^{-3}	5×10^{-5}
90	0	3.3×10^{-3}	5×10^{-5}
	Diebold Data		
60	-	-	6×10^{-5}
	This Experiment		
0	$.5 \times 10^{-4}$	2×10^{-3}	2.1×10^{-5}
30	$.8 \times 10^{-4}$	1×10^{-3}	1×10^{-5}
60	$.2 \times 10^{-4}$	1×10^{-3}	$.5 \times 10^{-5}$
90	$.2 \times 10^{-4}$	1×10^{-3}	3.0×10^{-5}

F. Statistical Errors

The errors discussed previously are given here together with typical values.

1) Counting statistics: 5 per cent on foreground, 3 per cent on background, and 2 per cent on accidentals.

2) Calibration error leading to error on counting rates of background and accidentals, 1 per cent.

3) Uncertainty in making cutoff between π^0 and $\pi^0\pi^0$ regions, 3 per cent.

G. Systematic Errors

Two sources of internal systematic error have been discussed. In Appendix V the contribution from single π^0's in pion-pair production is estimated to be less than 5 per cent of the measured cross section, and to decrease with increasing angle. In Section F. of this appendix it was estimated that the correction from energy variation of the cross section is less than 5 per cent, although possibly much larger.

Remaining sources of systematic error are related to the experimental work itself. 1) For the endpoint energy of the synchrotron, we have taken the value $E_0(\text{true}) = E_0(\text{set}) \times (1.023 \pm 0.003)$[14]. The detection efficiency changes by about 2 per cent per MeV, or a total error of about 6 per cent. This correction is independent of angle for each distribution to about 10 per cent. 2) The absolute normalization of the quantameter is estimated to be 2 per cent, with long term drifts of the same order. 3) The integrator calibration is measured to 2 per

TABLE 10

Run Configurations for Given Endpoint

Date	10/1-1/11	1/12-5/1		5/1-6/1	8/1-9/20	9/20-10/5	10/5-11/10
Radius	110	110	110	83	110	145	110
Aperture	5x7	6x7	8x7	6x7	6x8	6x8	6x8
Position #	1	2	3	4	5	6	5
Angle							
0	1308		1073			1513	
5	1308		1073			1513	
10	1308	1308	1073		1308	1513	
					1513		
15	1308	1308	1073		1308	1513	
					1513		
20	1308	1308	1073	1073	1308		1513
				1308	1513		
28		1308	1073	1073	1513		1308
			1308				1513
35		1308	1073	1073	1513		1513
			1308				
42			1308	1073			1513
56			1308	1073			1513

cent. These errors are considered in detail in Reference 3. The calculation of the detection efficiency has been discussed in Section E. An upper limit on the error is 1 per cent.

H. The Energy Dependence of the Cross Section

All of the information obtained by the experiment is contained in the spectrum S(E) itself. An attempt to unfold the energy dependence of the cross section from the data may be made with varying degrees of sophistication. An easily interpretable method is to fit the observed spectrum with a several parameter computed spectrum,

$$S_o(\delta_i) = \Sigma\, \alpha_n \int_i \int (E - E_o)^{n-1} Y(E) R(E, E') dE dE' .$$

As usual, we define

$$\chi^2 = \sum_{i=1}^{n} \frac{(S_o(\delta_i) - S(\delta_i))^2}{\sigma^2(\delta_i)}$$

and use least-squares method to find the α_n. We investigate this procedure numerically by generating spectra $S_o(\delta_i)$ for various cross sections, to see what errors $\Delta\alpha_n$ to expect. The resulting error matrix does not depend very strongly on the choice of cross section, allowing us to write

$$\Delta\alpha_1 \cong 0.08 \times \sqrt{1000/N}$$

$$\Delta\alpha_2 = 0.10 \times \sqrt{1000/N} \times 10^{-2}\ \mu b/MeV$$

$$\Delta\alpha_3 = 0.20 \times \sqrt{1000/N} \times 10^{-2}\ \mu b/MeV^2$$

where N is the total number of counts in the spectrum. Recalling the values estimated from the data for the cross-section parameters, $\alpha_2 = 0.3 \times 10^{-2}$, $\alpha_3 = 0.1 \times 10^{-4}$ and that $N < 1000$ counts, the difficulty of obtaining cross-section information is made apparent. We conclude the following:

1) χ^2 will be reasonable even for rapidly changing cross sections.

2) The sign of the slope α_2, and an idea of its magnitude, is obtainable. This will not, of course, change the mean cross section $\sigma(k_o, \theta_o)$.

3) The second derivative is unobtainable so no correction can be made to the data. This is true even for $\alpha_3 = 0.2 \times 10^{-4}$ μbarn/MeV^2, which would change the cross section by 0.1 μbarn, or 10 per cent.

4) The errors on the data $(\sigma_d - \sigma_p)$ are given by $N \cong 500$, so not even a slope may be reliably quoted.

There are two additional sources of error other than counting statistics on the coefficients α_n: 1) error in energy calibration of the two sides, and 2) error in the width of the response function $R(E, E')$. Since we are not going to try to obtain information from the deuterium data, we will not investigate these points.

APPENDIX III. COMPLETE COUNTING DATA

We present here the complete counting data of the experiment. Some of the points are the result of the combination of runs from different configurations. For presentation purposes, the rates and errors were normalized by use of the calculated efficiency ratio. The process of analysis made no attempt to combine background runs widely separated in time, which causes rates used for deuterium to differ slightly from those used for hydrogen. As discussed in Appendix II, the background rates for the small angle E_o = 1513 MeV data were time dependent, which accounts for the rather large difference here between the hydrogen and deuterium rates. The rates for the hydrogen runs are taken from Reference 3.

TABLE 11A COMPLETE COUNTING DATA
ENDPOINT = 1073.0 MEV

HYDROGEN

ANGLE	POSITION	FOREGROUND COUNTS	FOREGROUND BIPS	FOREGROUND RATE(ERROR)	CHISQ (RUNS)	BACKGROUND RATE(ERROR)	ACCIDENTAL RATE(ERROR)	ANALYSIS ERROR CALIB	ANALYSIS ERROR CUTOFF	PI ZERO RATE(ERROR)
0.	2	365	1000	0.365(0.019)	0.7(2)	0.082(0.010)	0.005(0.005)	0.000	0.006	0.278(0.023)
5.0	2	258	540	0.478(0.030)	3.6(2)	0.132(0.019)	0.003(0.004)	0.003	0.007	0.343(0.036)
10.0	2	420	703	0.597(0.029)	0.1(2)	0.182(0.030)	0.020(0.010)	0.008	0.000	0.395(0.044)
15.0	2	455	500	0.910(0.043)	0.4(2)	0.120(0.024)	0.010(0.010)	0.023	0.000	0.780(0.055)
21.0	4	668	560	1.193(0.046)	1.1(2)	0.117(0.022)	0.000(0.010)	0.011	0.016	1.076(0.056)
28.0	4	1697	1520	1.116(0.027)	4.6(4)	0.088(0.015)	0.033(0.010)	0.010	0.015	0.995(0.037)
35.0	4	2124	2144	0.991(0.021)	3.2(6)	0.095(0.013)	0.023(0.010)	0.013	0.017	0.873(0.035)
42.0	4	1108	1370	0.809(0.024)	3.2(5)	0.062(0.011)	0.014(0.010)	0.007	0.010	0.733(0.031)
49.0	4	1100	1814	0.606(0.018)	0.1(2)	0.072(0.013)	0.000(0.010)	0.005	0.007	0.534(0.026)

DEUTERIUM

ANGLE	POSITION	FOREGROUND COUNTS	FOREGROUND BIPS	FOREGROUND RATE(ERROR)	CHISQ (RUNS)	BACKGROUND RATE(ERROR)	ACCIDENTAL RATE(ERROR)	ANALYSIS ERROR CALIB	ANALYSIS ERROR CUTOFF	PI ZERO RATE(ERROR)
0.	2	583	500	1.166(0.048)	3.2(2)	0.082(0.010)	0.025(0.010)	0.011	0.085	1.059(0.099)
5.0	2	918	600	1.530(0.050)	1.7(2)	0.132(0.019)	0.061(0.020)	0.020	0.067	1.337(0.090)
10.0	2	1016	500	2.032(0.064)	4.0(3)	0.182(0.030)	0.020(0.010)	0.046	0.018	1.830(0.087)
15.0	2	1679	800	2.099(0.051)	5.3(2)	0.120(0.024)	0.012(0.011)	0.030	0.020	1.967(0.068)
21.0	4	1987	762	2.608(0.058)	3.6(3)	0.117(0.022)	0.000(0.010)	0.025	0.075	2.491(0.101)
28.0	4	2624	1137	2.308(0.045)	2.0(3)	0.088(0.015)	0.010(0.010)	0.031	0.055	2.210(0.080)
35.0	4	2350	1220	1.926(0.040)	0.5(3)	0.095(0.013)	0.056(0.020)	0.025	0.053	1.775(0.075)
42.0	4	1936	1216	1.592(0.036)	0.5(3)	0.062(0.011)	0.080(0.030)	0.015	0.029	1.450(0.058)
49.0	4	1054	924	1.141(0.035)	0.1(2)	0.072(0.013)	0.000(0.010)	0.011	0.043	1.069(0.059)

TABLE 11B COMPLETE COUNTING DATA
ENDPOINT = 1308.0 MEV

HYDROGEN

ANGLE	POSITION	FOREGROUND COUNTS	FOREGROUND BIPS	FOREGROUND RATE(ERROR)	CHISQ (RUNS)	BACKGROUND RATE(ERROR)	ACCIDENTAL RATE(ERROR)	ANALYSIS ERROR CALIB	ANALYSIS ERROR CUTOFF	PI ZERO RATE(ERROR)
0.	1	502	2100	0.239(0.011)	2.6(4)	0.067(0.008)	0.014(0.004)	0.002	0.005	0.158(0.015)
5.0	1	986	2850	0.346(0.011)	6.4(6)	0.072(0.012)	0.072(0.012)	0.003	0.005	0.202(0.021)
11.0	1	925	2000	0.462(0.015)	0.2(3)	0.056(0.004)	0.069(0.006)	0.005	0.002	0.337(0.018)
17.0	1	1337	3160	0.423(0.012)	0.7(3)	0.038(0.006)	0.013(0.005)	0.000	0.000	0.372(0.014)
23.0	1	1185	2987	0.397(0.012)	5.6(6)	0.038(0.003)	0.010(0.003)	0.000	0.003	0.349(0.013)
28.0	2	1109	3203	0.346(0.010)	2.2(6)	0.027(0.006)	0.010(0.007)	0.000	0.006	0.309(0.015)
35.0	2	698	3275	0.213(0.008)	2.6(7)	0.013(0.006)	0.004(0.003)	0.000	0.003	0.196(0.011)
42.0	3	390	2300	0.170(0.009)	5.7(5)	0.018(0.004)	0.000(0.000)	0.000	0.002	0.152(0.010)
49.0	3	340	3131	0.109(0.006)	4.9(6)	0.007(0.004)	0.000(0.000)	0.001	0.001	0.102(0.007)
56.0	3	358	4000	0.089(0.005)	9.0(6)	0.010(0.003)	0.000(0.000)	0.000	0.000	0.079(0.006)

DEUTERIUM

ANGLE	POSITION	FOREGROUND COUNTS	FOREGROUND BIPS	FOREGROUND RATE(ERROR)	CHISQ (RUNS)	BACKGROUND RATE(ERROR)	ACCIDENTAL RATE(ERROR)	ANALYSIS ERROR CALIB	ANALYSIS ERROR CUTOFF	PI ZERO RATE(ERROR)
0.	1	574	1500	0.383(0.016)	2.3(3)	0.067(0.008)	0.014(0.007)	0.003	0.006	0.302(0.020)
5.0	1	1113	1550	0.718(0.022)	0.5(3)	0.072(0.012)	0.120(0.060)	0.005	0.005	0.526(0.065)
11.0	1	2256	2000	1.128(0.024)	0.2(3)	0.056(0.004)	0.123(0.016)	0.028	0.019	0.949(0.045)
17.0	1	2142	2000	1.071(0.023)	3.4(3)	0.038(0.006)	0.120(0.040)	0.046	0.000	0.913(0.065)
23.0	1	2641	2974	0.888(0.017)	2.3(3)	0.038(0.003)	0.091(0.040)	0.038	0.000	0.759(0.058)
28.0	2	1387	2310	0.600(0.016)	5.5(4)	0.027(0.006)	0.014(0.010)	0.008	0.000	0.559(0.021)
35.0	2	516	1500	0.344(0.015)	0.1(2)	0.013(0.006)	0.026(0.010)	0.000	0.012	0.305(0.023)
42.0	3	608	1958	0.311(0.013)	3.3(5)	0.018(0.004)	0.000(0.010)	0.000	0.009	0.293(0.019)
49.0	3	363	1800	0.202(0.011)	3.5(4)	0.007(0.004)	0.006(0.006)	0.000	0.006	0.189(0.014)
56.0	3	200	1200	0.167(0.012)	0.2(2)	0.010(0.003)	0.000(0.000)	0.000	0.008	0.157(0.014)

TABLE 11C COMPLETE COUNTING DATA
ENDPOINT = 1513.0 MEV

HYDROGEN

ANGLE	POSITION	FOREGROUND COUNTS	FOREGROUND BIPS	FOREGROUND RATE(ERROR)	CHISQ (RUNS)	BACKGROUND RATE(ERROR)	ACCIDENTAL RATE(ERROR)	ANALYSIS ERROR CALIB	ANALYSIS ERROR CUTOFF	PI ZERO RATE(ERROR)
0.	5	172	1016	0.169(0.013)	2.3(4)	0.045(0.012)	0.000(0.010)	0.000	0.004	0.124(0.021)
5.0	5	239	751	0.318(0.021)	0.5(3)	0.092(0.030)	0.000(0.010)	0.000	0.009	0.226(0.039)
10.0	6	1050	1078	0.974(0.030)	5.0(5)	0.275(0.020)	0.200(0.018)	0.005	0.010	0.499(0.042)
15.0	6	871	1100	0.792(0.027)	1.2(4)	0.140(0.020)	0.030(0.020)	0.013	0.019	0.622(0.045)
21.0	6	621	1200	0.517(0.021)	1.5(3)	0.056(0.015)	0.010(0.010)	0.005	0.014	0.451(0.031)
26.0	6	321	1450	0.221(0.012)	3.8(4)	0.018(0.010)	0.000(0.010)	0.001	0.006	0.203(0.020)
32.0	6	141	1020	0.138(0.012)	0.4(2)	0.018(0.010)	0.000(0.010)	0.001	0.004	0.120(0.019)
39.0	6	164	1650	0.099(0.008)	1.5(3)	0.015(0.010)	0.000(0.000)	0.000	0.003	0.084(0.013)
46.0	6	138	1150	0.120(0.010)	0.1(2)	0.016(0.006)	0.000(0.000)	0.000	0.005	0.104(0.013)
53.0	6	134	1400	0.096(0.008)	0.6(2)	0.014(0.010)	0.000(0.000)	0.000	0.005	0.082(0.014)

DEUTERIUM

ANGLE	POSITION	FOREGROUND COUNTS	FOREGROUND BIPS	FOREGROUND RATE(ERROR)	CHISQ (RUNS)	BACKGROUND RATE(ERROR)	ACCIDENTAL RATE(ERROR)	ANALYSIS ERROR CALIB	ANALYSIS ERROR CUTOFF	PI ZERO RATE(ERROR)
0.	5	233	600	0.388(0.025)	0.4(3)	0.050(0.014)	0.060(0.025)	0.000	0.003	0.278(0.038)
5.0	5	256	400	0.640(0.040)	0.3(3)	0.092(0.030)	0.020(0.015)	0.002	0.013	0.528(0.054)
10.0	6	510	324	1.574(0.070)	0.3(3)	0.194(0.035)	0.062(0.023)	0.013	0.066	1.318(0.106)
15.0	6	1443	941	1.533(0.040)	2.7(4)	0.140(0.020)	0.030(0.015)	0.068	0.023	1.363(0.086)
21.0	6	740	800	0.925(0.034)	0.2(2)	0.056(0.015)	0.000(0.010)	0.009	0.026	0.869(0.047)
26.0	6	583	1125	0.518(0.021)	0.2(2)	0.018(0.010)	0.010(0.010)	0.001	0.015	0.490(0.030)
32.0	6	229	825	0.278(0.018)	0.8(2)	0.018(0.010)	0.015(0.015)	0.001	0.015	0.245(0.030)
39.0	6	313	1520	0.206(0.012)	0.3(3)	0.015(0.010)	0.020(0.010)	0.000	0.017	0.171(0.025)
46.0	6	115	640	0.180(0.017)	0.3(2)	0.016(0.006)	0.013(0.010)	0.000	0.005	0.151(0.021)
53.0	6	95	640	0.148(0.015)	0.3(2)	0.014(0.010)	0.010(0.010)	0.000	0.007	0.124(0.022)

TABLE 12A

CROSS SECTION DATA
K = 911 MEV

HYDROGEN

ANGLE LAB	ANGLE C M	MEAN K	DET EFF	COUNTING RATE(ERROR)	CROSS SECTION MICROBARNS/SR
0.	3.5	925	0.625	0.278(.023)	0.445(.037)
5.0	11.2	924	0.606	0.343(.036)	0.566(.060)
10.0	20.3	925	0.565	0.395(.044)	0.700(.077)
15.0	28.0	918	0.534	0.780(.055)	1.461(.103)
21.0	38.1	925	0.671	1.076(.056)	1.603(.083)
28.0	47.9	911	0.611	0.995(.037)	1.629(.061)
35.0	57.4	900	0.520	0.873(.035)	1.678(.067)
42.0	67.3	900	0.374	0.733(.031)	1.959(.083)
49.0	77.5	904	0.247	0.534(.026)	2.164(.106)

DEUTERIUM

ANGLE LAB	ANGLE C M	MEAN K	DET EFF	COUNTING RATE(ERROR)	CROSS SECTION MICROBARNS/SR	RATIO D2/H2
0.	3.5	925	0.753	1.059(.099)	1.406(.132)	3.161(.394)
5.0	11.2	924	0.730	1.337(.090)	1.831(.124)	3.237(.407)
10.0	20.3	925	0.681	1.830(.087)	2.688(.127)	3.841(.462)
15.0	28.0	918	0.643	1.967(.068)	3.056(.105)	2.093(.165)
21.0	38.1	925	0.809	2.491(.101)	3.080(.125)	1.921(.126)
28.0	47.9	911	0.736	2.210(.080)	3.001(.108)	1.842(.096)
35.0	57.4	900	0.627	1.775(.075)	2.833(.119)	1.688(.098)
42.0	67.3	900	0.451	1.450(.058)	3.218(.129)	1.642(.096)
49.0	77.5	904	0.298	1.069(.059)	3.591(.197)	1.660(.122)

TABLE 12B

CROSS SECTION DATA
K = 1182 MEV

HYDROGEN

ANGLE LAB	ANGLE C M	MEAN K	DET EFF	COUNTING RATE(ERROR)	CROSS SECTION MICROBARNS/SR
0.	3.7	1169	0.344	0.158(.015)	0.459(.043)
5.0	11.4	1167	0.337	0.202(.021)	0.599(.062)
11.0	21.4	1171	0.304	0.337(.018)	1.110(.058)
17.0	31.9	1175	0.263	0.372(.014)	1.415(.053)
23.0	41.8	1176	0.224	0.349(.013)	1.557(.057)
28.0	51.6	1180	0.227	0.309(.015)	1.362(.067)
35.0	61.6	1180	0.158	0.196(.011)	1.241(.069)
42.0	72.0	1189	0.147	0.152(.010)	1.031(.066)
49.0	81.6	1186	0.117	0.102(.007)	0.868(.062)
56.0	91.0	1189	0.090	0.079(.006)	0.883(.062)

DEUTERIUM

ANGLE LAB	ANGLE C M	MEAN K	DET EFF	COUNTING RATE(ERROR)	CROSS SECTION MICROBARNS/SR	RATIO D2/H2
0.	3.7	1169	0.415	0.302(.020)	0.728(.049)	1.584(.183)
5.0	11.4	1167	0.406	0.526(.065)	1.295(.161)	2.162(.350)
11.0	21.4	1171	0.366	0.949(.045)	2.591(.122)	2.334(.164)
17.0	31.9	1175	0.317	0.913(.065)	2.881(.206)	2.036(.164)
23.0	41.8	1176	0.270	0.759(.058)	2.812(.214)	1.806(.153)
28.0	51.6	1180	0.274	0.559(.021)	2.045(.078)	1.501(.094)
35.0	61.6	1180	0.190	0.305(.023)	1.602(.119)	1.291(.120)
42.0	72.0	1189	0.177	0.293(.019)	1.651(.106)	1.602(.145)
49.0	81.6	1186	0.141	0.189(.014)	1.338(.099)	1.541(.158)
56.0	91.0	1189	0.108	0.157(.014)	1.445(.133)	1.635(.190)

TABLE 12C

CROSS SECTION DATA
K = 1390 MEV

HYDROGEN

ANGLE LAB	ANGLE C M	MEAN K	DET EFF	COUNTING RATE(ERROR)	CROSS SECTION MICROBARNS/SR
0.	3.1	1382	0.200	0.124(.021)	0.621(.103)
5.0	10.5	1385	0.182	0.226(.039)	1.243(.213)
10.0	19.6	1384	0.411	0.499(.042)	1.214(.102)
15.0	29.6	1384	0.375	0.622(.045)	1.658(.120)
21.0	39.2	1384	0.333	0.451(.031)	1.356(.093)
26.0	49.6	1388	0.253	0.203(.020)	0.804(.078)
32.0	60.3	1385	0.203	0.120(.019)	0.592(.092)
39.0	70.2	1385	0.158	0.084(.013)	0.534(.082)
46.0	80.8	1388	0.106	0.104(.013)	0.981(.122)
53.0	90.7	1385	0.083	0.082(.014)	0.984(.167)

DEUTERIUM

ANGLE LAB	ANGLE C M	MEAN K	DET EFF	COUNTING RATE(ERROR)	CROSS SECTION MICROBARNS/SR	RATIO D2/H2
0.	3.1	1382	0.241	0.278(.038)	1.155(.159)	1.858(.401)
5.0	10.5	1385	0.219	0.528(.054)	2.408(.246)	1.937(.387)
10.0	19.6	1384	0.495	1.318(.106)	2.661(.213)	2.192(.254)
15.0	29.6	1384	0.452	1.363(.086)	3.017(.191)	1.820(.175)
21.0	39.2	1384	0.401	0.869(.047)	2.166(.118)	1.597(.140)
26.0	49.6	1388	0.305	0.490(.030)	1.608(.097)	2.000(.229)
32.0	60.3	1385	0.245	0.245(.030)	1.000(.121)	1.688(.333)
39.0	70.2	1385	0.190	0.171(.025)	0.898(.132)	1.681(.356)
46.0	80.8	1388	0.128	0.151(.021)	1.180(.164)	1.202(.224)
53.0	90.7	1385	0.100	0.124(.022)	1.244(.221)	1.264(.310)

APPENDIX IV. RESOLUTION FUNCTION CALCULATION

A. Yield of Pions in the Laboratory

We wish to compute the yield of pions in the laboratory from a deuteron target with a constant center-of-mass cross section. We consider here the modification of kinematics due to the internal motion of the nucleons and due to the binding energy of the deuteron. We define the 4-vectors by

k = photon energy in lab
p = target nucleon in lab
n = spectator nucleon in lab
π = recoil pion in lab
r = recoil nucleon in lab
s = recoil spectator in lab
b = binding energy of deuteron in lab
W = total cm energy

k* = photon energy in cm
p* = target nucleon in cm
etc.

and the angles by

$$\text{Cos}\theta = \underline{k} \cdot \underline{\pi}$$

$$\text{Cos}\delta = \underline{k} \cdot \underline{r}$$

$$\text{Cos}\beta = \underline{\pi} \cdot \underline{s}$$

We take the binding energy of the deuteron into account in the conservation of energy. Define

$$b = (\text{binding energy})/2$$
$$p_o = M_p - b$$
$$n_o = M_n - b$$
$$M_a = (M_n - M_p)/2$$
$$M = M_a - b,$$

so $M_d = 2M_a - 2b$, and

also $M_p = M_a - \epsilon = M + b - \epsilon = M + e$.

We shall always talk of the target particle as a proton.

We use the spectator model, which assumes that the matrix element describing the process T_{fi} is a function of W only, and is the same as the free nucleon matrix element for equal CM energy, and that the spectator nucleon does not contribute to the interaction except in conservation of energy, so the spectator momentum is unchanged, i.e., $\underline{s} = \underline{n}$. Except for the kinematic factors to be computed, then, the deuteron cross section is the sum of the free proton and free neutron cross sections. For momentum transfers larger than about twice the average internal momentum of the target nucleons, about 150 MeV, this result is obtained from the impulse approximation without multiple scattering corrections.

The invariant definition of the cross section for a two-body reaction, $\underline{k} + p \rightarrow \pi + r$, is

$$d\sigma = M_1 M_4 \int \frac{1}{\underset{\sim}{k} \cdot \underset{\sim}{p}} \delta(\pi^2 - \mu^2)\delta(r^2 - M_p^2)\delta^4(\pi + r - k - p) |T_{fi}|^2 d^4\pi d^4 r .$$

The quantity $\underset{\sim}{k} \cdot \underset{\sim}{p}$ is the usual flux factor $kE_p(1 + \beta_p)$ for $\underline{p} = 0$. We consider the change to $d\sigma(W)$ as a function of the target momentum $\underline{p}$. The total energy is

$$W^2 = (k + p)^2 = 2kM + M^2 - 2k \cdot p$$

and

$$\underset{\sim}{k} \cdot \underset{\sim}{p} = kM(1 + \frac{p}{M} \cos\theta)$$

but

$$kM = \frac{W^2 - M^2}{2(1 + \frac{p}{M} \cos\theta)} \qquad \text{so} \quad \underset{\sim}{k} \cdot \underset{\sim}{p} = (W^2 - M^2)/2$$

and doing the integrals over the delta functions, we have

$$d\sigma^* = \frac{1}{(\frac{W^2 - M^2}{2})} \times q_W \times \frac{M_p M_r}{2} \times |T_{f_L}|^2 \times d\Omega^*$$

so the center-of-mass cross section is not a function of the target momentum for a given total energy. The number of pions produced into the laboratory solid angle $d\Omega$ by $N(k)dk$ photons from $D(\underline{s})d^3\underline{s}$ nucleons is

$$dN = \frac{d\sigma}{d\Omega^*} \frac{d\Omega^*}{d\Omega} N(k)dk\, D(s)\, d^3s \ .$$

We take the parameters to be:

ω = pion energy

θ = pion angle in the laboratory

k_o = photon energy for production of a pion of energy ω at angle θ from a stationary target nucleon.

The energy spectrum of pions is

$$\frac{dN}{d\omega} = \int \frac{d\sigma}{d\Omega^*} \frac{d\Omega^*}{d\Omega} N(k) \frac{dk}{d\omega} D(\underline{s})\, d^3\underline{s}$$

evaluated for fixed (ω, θ) and integrated over the deuteron momentum distribution. The cross section quoted is defined from the total number of counts by

$$N = \left\langle \frac{d\sigma}{d\Omega^*} \right\rangle \int F(k, s, \theta)\, d\omega\, d^3\underline{s}$$

where

$$F(k, s, \theta) = \frac{d\Omega^*}{d\Omega} \frac{B(K)}{K} \frac{dK}{d\omega} D(\underline{s}) \ .$$

The procedure we use is to write for any kinematic variable $F(x) = F_o(x)(1 + \delta)$, where F_o is the value of the variable for pion production from a stationary target and δ is the correction which depends on the deuteron variables. The deuteron is parameterized in terms of the momentum and direction of the target nucleon $(\underline{s}, \theta, \varphi)$ and the kinetic energy $T = s_o - M$. Since $|\underline{s}| < 200$ MeV, the nucleon can be treated nonrelativistically, so $T = s^2/2M$.

1) For example, to solve for the lab photon energy we use

$$k + p + n = \pi + r + s$$

$$k = k_o \times \frac{1 + \epsilon_1}{1 + \epsilon_2} = k_o \times (1 + \epsilon)$$

$$\epsilon_1 = ((s_o - M)(2M - \omega) - \omega e + qs\cos\beta)/(\omega M_p - \mu^2/2)$$

$$\epsilon_2 = -((s_o - M - s\cos\delta) - e)/(M_p - \omega + q\cos\theta)$$

where

$$k_o = \frac{\omega M_p - \mu^2/2}{M_p - \omega + q\cos\theta}$$

is the value of photon energy, given (ω, θ) and a stationary proton target.

2) Center-of-mass energy,

$$W^2 = W_o^2 + \Delta$$

$$\Delta = \epsilon(W_o^2 - M_p)^2 - (2k_o + 2\epsilon k_o - 2M_p)e - s^2 + 2(k_o + \epsilon k_o)s\cos\delta .$$

3) Solid angle transformation $(d\Omega^*/d\Omega) \times dk/d\omega$, for the invariant I,

$$\frac{dI}{d\Omega^{d\omega}/dk} = \frac{dI}{d\Omega^{d\omega}/dk}\Bigg|_o /(1+\eta)$$

$$\eta = k_o(sCos - e - (s_o - M_p))/(\omega M_p - \mu^2/2$$

$$\frac{d\Omega^*}{dI} = \frac{d\Omega^*}{dI}\Bigg|_o (1+\Delta)$$

Define

$$n = M_p + \mu \qquad d = M_p - \mu$$

$$m_1 = \frac{1}{W_o^2 - n^2} \qquad m_2 = \frac{1}{W_o^2 - d^2} \qquad m_3 = \frac{1}{W_o^2}$$

$$d = \omega M_p - \mu^2/2$$

$$A_\Delta = m_3 - \frac{m_1 + m_2}{2} \qquad B_\Delta = \frac{3}{8}(m_1^2 + m_2^2) - \frac{m_1 m_2 + m_2 m_3}{2}.$$

Then

$$\Delta = \alpha_1 + \alpha_2 \cos\beta + \alpha_3 \cos\delta + \alpha_4 \cos^2\beta + \alpha_5 \cos^2\delta + \alpha_6 \cos\beta \cos\delta$$

$$\ell = \omega M - \mu^2/2$$

$$\alpha_1 = A_\Delta S^2 \left[\frac{R_0(2M - \omega + k_0)}{\ell} - 1 \right] - 2A_\Delta (k_0 - M)\epsilon$$

$$\alpha_2 = A_\Delta S^2 \left[\frac{2k_0 M q}{\ell} \right]$$

$$\alpha_3 = A_\Delta \times 2k_0 S \left[1 - \frac{Mk_0}{\ell} \right]$$

$$\alpha_4 = B_\Delta S^2 \left[\frac{4k_0^2 M^2 q^2}{\ell^2} \right]$$

$$\alpha_5 = A_\Delta \times 2k_0 S^2 \left[\frac{k_0 M}{\ell^2} - \frac{1}{\ell} \right] + B_\Delta \times 4k_0^2 \left[S - MD\epsilon \right]^2 + B_\Delta \times 4k_0^2 S^2 \left[1 - \frac{Mk_0}{\ell} \right]^2$$

$$\alpha_6 = A_\Delta \times 2k_0 S^2 \left[q/\ell - \frac{Mqk_0}{\ell^2} \right] + B_\Delta \times 8k_0^2 M S^2 \left[q/\ell - \frac{Mqk_0}{\ell^2} \right]$$

So we finally have

$$F = \frac{1}{k} \frac{d\Omega^*}{d\Omega} \frac{dk}{d\omega} = F_0 \times \left(\frac{1+\epsilon_2}{1+\epsilon_1} \right) \times (1+\Delta) \times \frac{1}{1+\eta} \quad .$$

Next we write

$$\epsilon_1 = A_\epsilon + B_\epsilon \cos\beta$$

$$\epsilon_2 = C_\epsilon + D_\epsilon \cos\delta$$

$$\eta = A_\eta + B_\eta \cos\delta \ .$$

We take

$$s = 100 \text{ MeV}, \quad s_o - M = 10 \text{ MeV}$$

$$\omega = k = 1000 \text{ MeV}, \quad W^2 = 3 \times 10^6 \text{ MeV}^2$$

to get

$$A_\Delta = 1/6 \times 10^{-6} \qquad B_\Delta = 1/5 \times 10^{-3}$$

and with the order of the correction terms

$$A_\epsilon \sim T/M \qquad B_\epsilon \sim S/M \qquad C_\epsilon \sim T/M \qquad D_\epsilon \sim S/M$$

$$A_\eta \sim T/M \qquad B_\eta \sim S/M \ .$$

We expand to find

$$\epsilon = A_\epsilon - C_\epsilon + B_\epsilon \cos\beta - D_\epsilon \cos\delta$$

$$+ D_\epsilon^2 \cos^2\delta - B_\epsilon D_\epsilon \cos\beta \cos\delta$$

and $1/(1+\eta) = 1 - \eta + \eta^2$ keeping terms which are $0(10^{-4})$.

Combining all the binding energy terms gives

$$G_B = \left(\frac{\omega}{d} - 2A_\Delta(k_o - M)\right)e$$

or $G_B \sim e/M = 10^{-3}$ so we are justified in keeping only the first order terms. Since $D(\underline{s})$ is isotropic, $D(\underline{s})d^3s = D(|\underline{s}|)ds d\Omega_\delta$. We also observe that the integrals $\int \cos\delta\, d\Omega_\delta = \int \cos\beta\, d\Omega_\delta = 0$. To order 10^{-4},

$$F = F_o \times (1 + f)$$

$$f = G_B - A + \alpha_1 + \frac{1}{3}(B^2 - B\alpha_2 + \alpha_4 + \alpha_5) + \frac{1}{3}\cos\theta\,(\alpha_6 - B\alpha_3).$$

Thus we have the yield of pions in the laboratory

$$dN = Y_o(1 + f) \times \left\langle \frac{d\sigma}{d\Omega^*} \right\rangle \times d\omega \times D(|\underline{s}|)ds$$

where $Y_o = \frac{d\Omega^*}{d\Omega}\frac{dk}{d\omega}\frac{B(k)}{k}$ evaluated for stationary target kinematics. Since f depends linearly on s and s^2, we can do the integral over s, $\int f D(s)\, ds$ by replacing s by $\langle s \rangle$ and s^2 by $\langle s^2 \rangle$ to obtain $Y = Y_o \times \int (1 + f)\, D(s) ds$.

B. Acceptance Function

In this section we compute the number η, which connects the counting rate with a constant center-of-mass cross section. We also define the mean angle and energy k_o and θ_o, and discuss the magnitude of error expected in equating $\bar{\sigma}(k_o, \theta_o)$ with $\sigma(k_o, \theta_o)$. The observable spectrum shape is also calculated. We define

$Y(E,\theta)$	=	Yield of pions in the lab from a constant CM cross section, including the shape of the photon energy spectrum
C	=	Counting rate
k	=	Photon energy
E	=	Pion energy
E_1, E_2	=	Energy of the decay gamma rays
E_1', E_2'	=	Output of counters using energy scale
$R(E_1', E)$	=	Resolution function of Cherenkov counter.

A quantity in the CM frame will be denoted by an *, e.g., k* = photon energy in CM. The following functions are useful:

1) $T(k^*,\theta^*)$, the energy-angle resolution function in the CM for pions detected by the counter in terms of the quantities in which the cross section is usually given;

2) $(E,\theta,\varphi,\underline{r})$, the probability of detecting a pion given by (E,θ,φ) produced at a point $\underline{r}$ in the target;

3) $V(E_1, E_2, \theta)$, the distribution of gamma-ray energies of detected pions at given angle θ;

4) η (configuration), the number which connects counting rate with the constant center-of-mass cross section, defined by $C = \eta \times d\sigma/d\Omega^*$. To find these functions analytically would require solving for a function $\Phi(E, \theta, \varphi, E_1, E_2, k, \underline{r})$. Such a function is impossible to compute in practice, so we turn to two approximate methods. By use of a Monte Carlo program, the experiment may be duplicated on the computer to some statistical accuracy. The events are tallied by the parameters of interest. Clearly, all the functions above may be generated in this manner to an accuracy limited only by the amount of computer time available. The program for the configuration used by this experiment obtained about 1500 successes per minute. An approximate analytic function for η has been derived[2] which, when compared with the Monte Carlo program, is of sufficient accuracy for most calculations. The advantage of this function is that a complete calculation may be done in about five seconds.

The functions T and ϵ define η immediately,

$$\eta = \int T(k^*, \theta^*)\, dk^*\, d\theta^*$$

$$= \int Y(E, \theta)\, \epsilon(E, \theta)\, dE d\theta$$

which also relate T and ϵ,

$$T(k^*, \theta^*) = Y(E, \theta)\, \epsilon(E, \theta) J\left(\frac{E, \theta}{k^*, \theta^*}\right).$$

Defined in this manner $T(k^*, \theta^*)$ includes the photon spectrum and the deuteron variables (a small correction to the free nucleon case) while $\epsilon(E, \theta)$ does not. The counting rate in terms of T is given by

$$C = \int \sigma(k^*, \theta^*)\, T(k^*, \theta^*)\, dk^* d\theta^*$$

so the quoted cross section is

$$\bar{\sigma}(k_o^*, \theta_o^*) = C/\eta$$

if k_o^* and θ_o^* are the expectation values defined by T,

$$k_o^* = \langle k^* \rangle = \frac{1}{\eta} \int k^* T(k^*, \theta)\, dk^*\, d\theta \quad .$$

The Monte Carlo program will calculate these numbers easily.

Next we consider the two dimensional distribution of gamma ray energies $V(E_1, E_2)$. The observed matrix will use the response functions of each counter giving

$$O(E_1', E_2') = \int V(E_1, E_2) R_1(E_1', E_1) R_2(E_2', E_2) dE_1 dE_2$$

where R_1 and R_2 are Gaussian with widths $\varkappa_1$ and $\varkappa_2$. We wish the distribution of $E' = E_1' + E_2'$

$$F(E' = E_1' + E_2') = \int O(E' - E_2',\ E_2') dE_2' \quad .$$

The convolution of the two Gaussians gives

$$F(E') = \frac{1}{\sqrt{2\pi}} \int \frac{V(E_1, E_2)}{(\varkappa_1 E_1 + \varkappa_2 E_2)} \exp - \frac{(E' - (E_1 + E_2))^2}{2(\varkappa_1 E_1 + \varkappa_2 E_2)} \, dE_1 dE_2 \ .$$

The widths of the two response functions were measured to be

$$\varkappa_1 = 4.55 \text{ MeV (220 p.e.)} \quad \varkappa_2 = 5.26 \text{ MeV (180 p.e.)}.$$

Let

$$E = E_1 + E_2 \quad \varkappa = \frac{\varkappa_1 + \varkappa_2}{2} = 4.90$$

$$\Delta = E_1 - E_2 \quad \delta = \frac{\varkappa_1 - \varkappa_2}{2} = 0.35 \ .$$

Then

$$F(E') = \frac{1}{\sqrt{2\pi}} \int V(E_1, E_2)(\varkappa E + \delta \Delta)^{-1} \exp - \frac{(E' - E)^2}{(2\varkappa E + 2\delta \Delta)} \, dE_1 dE_2 \ .$$

Taking typical values for the variables,

$$E = 1000 \text{ MeV} \quad \Delta < 600 \text{ MeV}, \quad \varkappa E = (70 \text{ MeV})^2$$

so $(E' - E) \approx 200$ MeV. Then

$$\frac{1}{\kappa E}\left(1+\frac{\delta\Delta}{\kappa E}\right)^{-1} \cong \frac{1}{\kappa E}\left(1-\frac{\delta\Delta}{\kappa E}+\frac{1}{2}\left(\frac{\delta\Delta}{\kappa E}\right)^{2}\right)$$

so the exponential term is

$$\frac{1}{\kappa E}\left(1-\frac{\delta\Delta}{\kappa E}+\frac{1}{2}\left(\frac{\delta\Delta}{\kappa E}\right)^{2}\right) \exp -\frac{(E'-E)^{2}}{2\kappa E} \times \exp -\frac{(E'-E)^{2}}{2\kappa^{2}E^{2}}\delta\Delta \ .$$

The counters are symmetric with respect to the production plane, so $V(E_1, E_2) = V(E_2, E_1)$. Noting $\Delta \rightarrow -\Delta$ the exponential is then

$$\frac{1}{\kappa E}\exp -\frac{(E'-E)^{2}}{2\kappa E}\left[1+\frac{1}{2}\left(\frac{\delta\Delta}{\kappa E}\right)^{2}\right]\cosh\left(\frac{(E'-E)^{2}}{2\kappa^{2}E^{2}}\delta\Delta\right) \ .$$

The typical values give $\frac{1}{2}\left(\frac{\delta\Delta}{\kappa E}\right)^{2} = 0.001$ and $\cosh\left(\frac{(E'-E)^{2}}{2\kappa^{2}E^{2}}\delta\Delta\right) =$ $1 + .05$. The Monte Carlo program shows that, in fact, 90 per cent of the successes have $\Delta < 200$ MeV, so the correction term is less than 2 per cent. The actual spectrum obtained will be

$$F(E') = \int V(E_1, E_2) \exp -\frac{(E' - (E_1 + E_2))^{2}}{2\kappa(E_1 + E_2)} dE_1 dE_2 \ .$$

Using the definition of $S(E)$ in terms of V, $S(E) = \int V(E - E_2, E_2)dE_2$. We obtain for the observed energy spectrum

$$F(E') = \int S(E)\, \exp^{-(E' - E)^2/2\varkappa E}\, dE \ .$$

We next derive the parameters of the observed spectrum in terms of the cross section and the parameters of the resolution function. Since

$$\sigma(k) = \sigma(k_o) + \frac{\partial \sigma}{\partial k}(k - k_o) + \frac{1\partial^2 \sigma}{2\partial k^2}(k - k_o)^2$$

and $E - E_o = \frac{\partial E}{\partial k}(k - k_o)$, we have

$$\sigma(E) = \sigma_o + \beta(E - E_o) + \gamma(E - E_o)^2 \ .$$

For the resolution function $Y(E)$ we have $\int Y(E)dE = 1$, $E_o = \int EY(E)dE$, $\sigma_Y^2 = \int (E - E_o)^2 Y(E)dE$, $S_Y^3 = \int (E - E_o)^3 Y(E)dE$. Then from $S(E') = \int \sigma(E, E_o) Y(E) R(E, E')dE$ we have

$$\int S(E')dE' = \alpha + \gamma\, \sigma_Y^2 = \mu$$

and

$$\langle E' = E_o \rangle = \frac{\beta}{\mu}\, \sigma_Y^2 + \frac{\gamma}{\mu}\, S_Y^3$$

$$\langle E' \rangle = E'_o = E_o + \frac{\beta}{\mu}\sigma_Y^2 + \frac{\gamma}{\mu}\, S_Y^3 \ .$$

After some algebra, $\sigma'^2 = \langle (E' - E'_o)^2 \rangle = \frac{\alpha}{\mu}\, \sigma_Y^2 + kE_o + k(\frac{\beta}{\mu}\sigma_Y^2 + \frac{\gamma}{\mu} S_Y^3)$

$+\frac{\beta}{\mu} S_Y^3 + \frac{\gamma}{\mu} q_Y^4 - (\frac{\beta}{\mu}\sigma_Y^2 + \frac{\gamma}{\mu} S_Y^3)^3$. A corollary of this formula is obtained by setting $\alpha = 1$, $\beta = \gamma = 0$, showing that the convolution of a distribution $Y(E)$ of mean E_o and width σ_Y with a Gaussian response function of mean E, and width $\varkappa E$ gives a distribution of mean E_o, width $\sigma'^2 = \sigma_Y^2 + kE_o$. For an estimate of the size of the corrections, we take the values again at 20 degrees, $k_{max} = 1500$ MeV, $\sigma_Y^2 = 5.0 \times 10^3$ MeV^2, $S_Y^3 = -3.5 \times 10^4$ MeV^3, $|\beta| = \frac{\partial\sigma}{\partial k}\frac{\partial k}{\partial E} = 10^{-2}$, $|\gamma| = 10^{-4}$ for which we obtain $E_o - E'_o = 35$ MeV and $\sigma'^2 = 8420 = \sigma_o^2 - 2380$. Since $\sigma_o = 104$ MeV, then $\sigma' = 92$ MeV. Taking the values estimated from data we obtain $E_o - E'_o = 10$ MeV and $\sigma'^2 = 101$ MeV. We apparently will find good agreement between observed and computed values for slowly varying cross sections.

For plotting purposes we also have the spectrum in each counter,

$$I(E) = \int U(E_1 E_2)dE$$

and the spectrum in $\Delta = E_1 - E_2$

$$D(\Delta) = \int U(\Delta + E_2, E_2)dE_2 \ .$$

Note that the moments

$$\sigma_S^2 = \sigma_A^2 + \sigma_B^2 + \langle (E - E_H^o)(E - E_B^o)\rangle$$

and

$$\sigma_D^2 = \sigma_A^2 + \sigma_B^2 - \langle (E - E_A^o)(E - E_B^o) \rangle$$

define the correlation coefficient for the matrix.

APPENDIX V. PION PAIR CORRECTIONS

A. Detection of single π^o's in the reaction $\gamma + N \rightarrow \pi^o + (\pi N')$

We choose the parameters of this reaction to be (E_{π^o}, k, θ_π, M_Δ), where $M_\Delta^2 = (E_\pi + E_{N'})^2 - P_\pi \cdot P_{N'}$ is the invariant mass of the pion nucleon system. Figure 19 shows this mass as a function of E_π for various photon energies. The cross section is given by $\frac{d^2\sigma}{d\Omega dE} = \frac{q}{k} \times \frac{1}{W} \times f(M_\Delta^2)|M|^2$ where

$$f(\Delta^2) = \frac{1}{\Delta^2}\left[(\Delta^2 - (M_\rho - M_\pi)^2)(\Delta^2 - (M_\rho + M_\pi)^2)\right]^{1/2}$$

and $|M|^2$ is the sum over all the contributing matrix elements. We compute with two models:

1) The statistical model, in which $|M|^2$ is taken to depend on only W, and found from the total cross section.

2) The resonant production model, in which the cutoff on pion energy requires M_Δ be near the mass of the first resonance $N_1^*(1238)$, and the mechanism of production to be $\gamma + N \rightarrow \pi^o + N^*$. The matrix element then has a Breit-Wigner shape $|M|^2 = \frac{\alpha^2\Gamma^2}{[(M_\Delta - M_R)^2 + \Gamma^2]}$.

The reaction $\gamma + p \rightarrow \pi^o + (\pi + N)$ has not been measured, much less the corresponding reaction from deuterium. We have measurements

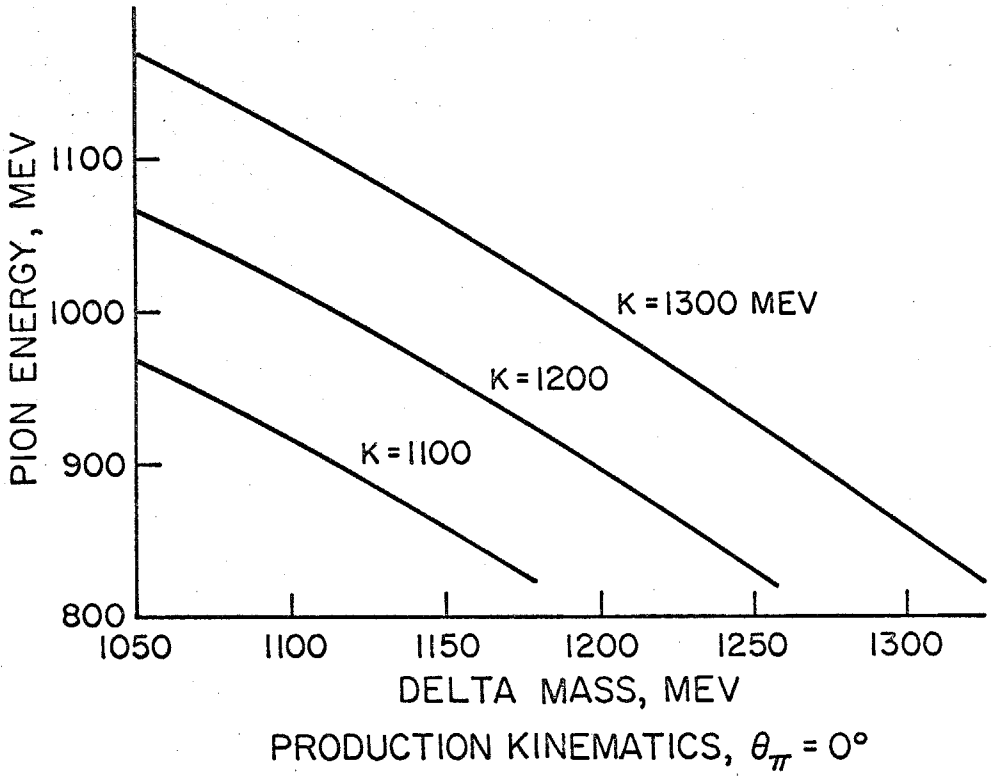

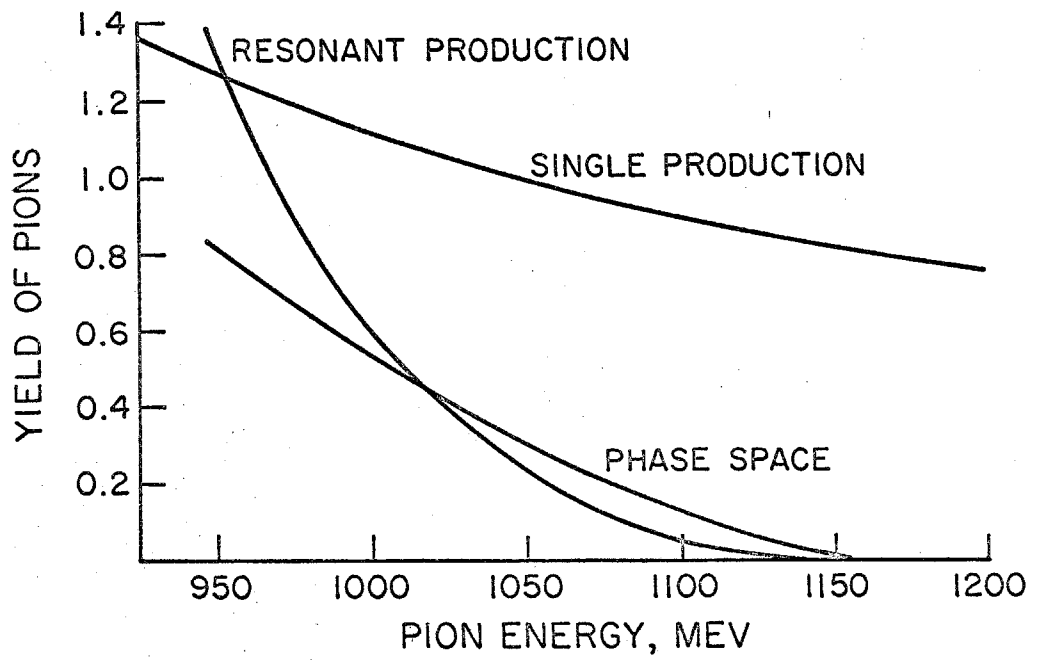

FIGURE 19 PION PAIR PRODUCTION

only of $\gamma + p \rightarrow \pi^+ + \pi^- + p$ with total cross sections, and of $\gamma + p \rightarrow \pi^- + N^*(1238)$, production of a pion and the first pion-nucleon resonance, with differential cross sections. As an upper limit, we take the cross sections for the corresponding π^o reactions from deuterium to be equal to 5 times these. It is impossible to justify this, but there are several plausibility remarks. 1) Pion production by pions[15] give comparable cross sections for all final states. The ratio $(\pi^- p \rightarrow \pi^- \pi^o p)/(\pi^- p \rightarrow \pi^+ \pi^- n) = 1/2$ favors the charged mode. 2) Calculation from isospin in the decay of a pure $T = 1/2$ state into a $T = 3/2$ state plus a pion, e. g., $N^*(1688) \rightarrow N^*(1238) + \pi$, gives a ratio of 2/3 favoring the charged mode. 3) The one pion exchange, or Drell, diagram for two pion production is small for a π^o in the forward direction. Using the results for the charged reactions, Table 12 for π^o's was calculated.

The experiment provided two checks on multiple pion production. 1) Synchrotron subtractions at (40^o, 1170) give a correction of (3.0 ± 3.0) per cent. Most of the statistical uncertainty arises from the difficulty in subtracting off the contribution from π^o production. 2) Fitting the observed spectrum to the computed spectrum shows there is no enhancement of the low energy side. The procedure will be inexact because of calibration uncertainty and difficulty in subtracting off the $\pi^o \pi^o$ events. An upper limit can be found of about 0.05 μbarns, which is a correction of 20 per cent at 0^o and 3 per cent at 40^o.

TABLE 13

Pion Pair Production Corrections

σ_T = 200 microbarns

1. E_o = 1070 MeV

Angle, Lab	Angle CM	Relative Phase Space	Cross Section Ratio Cross Section Resonant Production	Ratio, Phase Space	$\gamma^{+d}_{\rightarrow\pi^+(\pi N)} / \gamma^{+d}_{\rightarrow\pi^+d}$ Resonant Production
0.0	0.0	0.22	0.16	0.16	0.11
	30.0	0.14	0.12	0.047	0.040
	60.0	0.10	0.05	0.033	0.017
	90.0	0.04	0.02	0.001	0.001

2. E_o = 1308 MeV

	0.0	0.062	0.048	0.075	0.058
	30.0	0.042	0.030	0.015	0.010
	60.0	0.022	0.011	0.014	0.007
	90.0	0.001	0.000	0.001	0.000

3. E_o = 1510 MeV

	0.0	0.040	0.042	0.028	0.030
	30.0	0.031	0.031	0.011	0.011
	60.0	0.011	0.008	0.011	0.008
	90.0	0.002	0.000	0.002	0.000

REFERENCES

1. Henry Ruderman, Ph. D. Thesis, California Institute of Technology (1962).
2. R. M. Talman, Ph. D. Thesis, California Institute of Technology (1963).
3. G. L. Hatch, Ph. D. Thesis, California Institute of Technology (1967).
4. H. Ruderman, R. Gomez, and A. V. Tollestrup, California Institute of Technology Report CTSL - 31, unpublished (1962).
5. S. D. Ecklund, Private Communication.
6. J. M. Sellen, G. Cocconi, V. Cocconi, and E. L. Hart, Phys. Rev. 110, 779 (1958).
7. M. G. Hauser, Private Communication.
8. G. Chew and H. Lewis, Phys. Rev. 84, 779 (1951).
9. M. Goldberger and K. M. Watson, Collison Theory, Wiley, 1964, pp. 679-780.
10. J. Chapplear, Phys. Rev. 99, 254 (1955).
11. Chelton and Mann, "Cryogenic Data Book", UCRL - 3421 (1956).
12. H. A. Thiessen, "A Recalibration of the Beam Energy Meter", CTSL Internal Report No. 21, unpublished (1966).

13. R. Diebold, Ph. D. Thesis, California Institute of Technology (1963).

14. H. Thiessen, Ph. D. Thesis, California Institute of Technology (1967).

15. E. Pickup, D. Robinson, and E. O. Salant, Phys. Rev. Letters 7, 192 (1961).

16. T. Chang, Ph. D. Thesis, California Institute of Technology (1962).

17. H. Bingham, Ph. D. Thesis, California Institute of Technology (1960).